

# Shear viscosity of a hadronic gas mixture

Kazunori Itakura,<sup>1</sup> Osamu Morimatsu,<sup>1,2</sup> and Hiroshi Otomo<sup>2</sup>

<sup>1</sup>High Energy Accelerator Research Organization (KEK), Oho 1-1, Tsukuba, Ibaraki, 305-0801, Japan

<sup>2</sup>Department of Physics, University of Tokyo, 7-3-1 Hongo Bunkyo-ku Tokyo 113-0033, Japan

(Dated: November 7, 2007)

We discuss in detail the shear viscosity coefficient  $\eta$  and the viscosity to entropy density ratio  $\eta/s$  of a hadronic gas comprised of pions and nucleons. In particular, we study the effects of baryon chemical potential on  $\eta$  and  $\eta/s$ . We solve the relativistic quantum Boltzmann equations with binary collisions ( $\pi\pi$ ,  $\pi N$ , and  $NN$ ) for a state slightly deviated from thermal equilibrium at temperature  $T$  and baryon chemical potential  $\mu$ . The use of phenomenological amplitudes in the collision terms, which are constructed to reproduce experimental data, greatly helps to extend the validity region in the  $T$ - $\mu$  plane. The total viscosity coefficient  $\eta(T, \mu) = \eta^\pi + \eta^N$  increases as a function of  $T$  and  $\mu$ , indirectly reflecting energy dependences of binary cross sections. The increase in  $\mu$  direction is due to enhancement of the nucleon contribution  $\eta^N$  while the pion contribution  $\eta^\pi$  diminishes with increasing  $\mu$ . On the other hand, due to rapid growth of entropy density, the ratio  $\eta/s$  becomes a decreasing function of  $T$  and  $\mu$  in a wide region of the  $T$ - $\mu$  plane. In the kinematical region we investigated  $T < 180$  MeV,  $\mu < 1$  GeV, the smallest value of  $\eta/s$  is about 0.3. Thus, it never violates the conjectured lower bound  $\eta/s = 1/4\pi \sim 0.1$ . The smallness of  $\eta/s$  in the hadronic phase and its continuity at  $T \simeq T_c$  (at least for crossover at small  $\mu$ ) implies that the ratio will be small enough in the deconfined phase  $T \gtrsim T_c$ . There is a nontrivial structure at low temperature and at around normal nuclear density. We examine its possible interpretation as the liquid-gas phase transition.

## I. INTRODUCTION

Shear viscosity of a hot QCD matter has been attracting much attention in recent years. The major reason for that is the intriguing experimental discovery that the matter created in heavy-ion collisions at Relativistic Heavy Ion Collider (RHIC) in Brookhaven National Laboratory could be close to a perfect fluid [1]. This unexpected result has driven people to think about *strongly-interacting* quark-gluon plasma (abbreviated as “sQGP”) which may be realized at temperature just above the critical temperature  $T \gtrsim T_c$ . As a result of strong-coupling nature, sQGP is thought to have very small shear viscosity, which is however not directly confirmed yet in a satisfactory way. In fact, only a few things are understood about sQGP because we will not be able to investigate it within standard perturbative QCD techniques. The only technique available now (except for lattice simulations which are not analytic methods) is the one based on the AdS/CFT correspondence, which relates strongly-coupled supersymmetric Yang-Mills theories to weakly-coupled gravity theories.

There is an interesting outcome from the AdS/CFT analysis in relation to the shear viscosity: It has been conjectured that there would be a lower bound in the “shear viscosity coefficient to the entropy density ratio” (or simply the “viscosity to entropy ratio”)  $\eta/s \geq 1/4\pi$  [2]. We call this “the KSS bound” after authors’ names of Ref. [2]. The lowest value  $\eta/s = 1/4\pi$  is satisfied by several super Yang-Mills theories in the large  $N_c$  limit (strong coupling limit), which suggests that the bound could be universal. Of course, there is no guarantee for this bound to hold in real (non-supersymmetric) QCD whose gravity dual

is not found, but interestingly enough, the values of  $\eta/s$  extracted from RHIC experiments [3] and from lattice simulations [4, 5] seem to be small enough and close to the lower bound.

On the other hand, there is an important empirical observation which can be seen in many substances such as helium, nitrogen, and water: The ratio  $\eta/s$  has a minimum at or near the critical temperature [6] (see also [7]). More precisely, the ratio shows a cusp at  $T_c$  for the first order transition, while it has a convex shape for the crossover with its bottom around the (pseudo) critical temperature. Since this behavior is observed in many substances, it is expected to be universal. Recall that the phase transition in QCD is most probably crossover at least for low densities. Therefore, what we naturally expect for the QCD matter from the two observations mentioned above is that the ratio  $\eta/s$  will have the minimum at  $T \sim T_c$ , and the numerical value at that point will be close to the KSS bound  $\eta/s \sim 0.1$ . It is of primary importance to check whether this expectation is indeed the case or not, and to understand the properties of the QCD matter around  $T_c$  not only for  $T \gtrsim T_c$ . These considerations motivated us to investigate the shear viscosity in QCD *from the hadronic phase*  $T \lesssim T_c$ . Notice that we can indirectly study the properties of sQGP from below  $T_c$  because physical quantities such as the ratio  $\eta/s$  will be continuous at  $T_c$  for the crossover transition.

Transport properties of a meson gas have been studied by several people. Many of the calculations are based on the Boltzmann equations with the Chapman-Enskog method which is a standard approach for weak dissipative phenomena, especially for computing transport coefficients [8]. Differences among several papers

[9, 10, 11, 12, 13] include kinetic or statistical properties of particles (relativistic or nonrelativistic, quantum or classical), species of mesons (pions, kaons, etc.), and the cross sections in the collision terms. For example, Ref. [12] treated a nonrelativistic quantum pion gas with the binary cross section given by the leading order chiral perturbation theory (LO-ChPT). Recently, similar problems have been revisited in relation to the KSS bound [14, 15]. In Ref. [14], the ratio  $\eta/s$  computed with the cross section in LO-ChPT turned out to violate the KSS bound for temperature beyond  $T_c \sim 170$  MeV, and it was speculated that such violation could be related to the existence of phase transition. However, soon after that, it was shown in Ref. [15] that the KSS bound is not violated in a pionic gas if one computes the shear viscosity with a phenomenological cross section using the experimental phase shifts. What we have learned from these papers is the following: (i) we have to be careful when we use the cross section from effective field theories, and (ii) the ratio  $\eta/s$  of a relativistic pion gas is small enough at relatively large temperature  $T \lesssim T_c$ , but does not violate the KSS bound  $\eta/s \geq 1/4\pi$ .

At this point, there comes a natural question: how does  $\eta/s$  change if one adds nucleons to the pure pion gas? Naively, we expect that the ratio  $\eta/s$  will *decrease* as number of nucleons is increased because the pion cross section will effectively enhance in the presence of nucleons, yielding smaller shear viscosity, while the entropy will increase. Thus, there is a chance that the ratio could violate the KSS bound if the bound does not change. Notice that the pion-nucleon gas is the minimum requisite which allows us to study the effects of *baryon chemical potential*  $\mu$ . Therefore, it is quite interesting and important to investigate the  $\mu$  dependence of  $\eta/s$  in the pion-nucleon gas. Such investigation will also urge people to study the (possible)  $\mu$ -dependence of the KSS bound. In fact, the ‘‘universality’’ of the KSS bound has not been tested at finite baryon chemical potential.

Most recently, the authors of Ref. [14] have applied their framework to the pion-nucleon gas to study the behavior of  $\eta/s$  in the  $T$ - $\mu$  plane [16]. However, their focus was not on the KSS bound but on the new finding: a valley structure in  $\eta/s$  at low temperature and large chemical potential which they argued would correspond to the nuclear liquid-gas phase transition. Although this is a very interesting suggestion, their results should be critically checked since they are based on the effective field theories whose validity region is severely limited. On the other hand, a realistic calculation of the viscosity in the pion-nucleon gas was performed some time ago by Prakash et al. [10]. Remarkably, they used the binary cross sections in the collision terms, which roughly reproduce experimental data. However, unfortunately, the dependence on baryon chemical potential was not investigated in detail. Besides, this calculation is based on *classical* Boltzmann equations, and thus cannot be applied to relatively large chemical potential where the effects of Fermi statistics is expected to be large.

In view of the present situation mentioned above, what

we should do is rather evident: for the purpose of studying the  $\mu$  dependence of the shear viscosity  $\eta$  and the ratio  $\eta/s$  in a pion-nucleon gas, we treat the relativistic quantum Boltzmann equations with binary cross sections which are determined to reproduce experimental data. We are very careful about the range of validity of our framework. We also check whether the valley structure found in Ref. [16] indeed exists even with the phenomenological cross sections. It is also important to compare our results with those from hadron cascade simulations. For example, the shear viscosity coefficient is computed for a meson gas in Ref. [17] and for a meson-baryon gas in Ref. [18].

The paper is organized as follows: in the next section, we explain the relativistic quantum Boltzmann equations for a dilute pion-nucleon gas, and define the cross sections we use in the collision terms. We treat the small deviation from the thermal equilibrium to the linear order (the Chapman-Enskog method), and give the shear viscosity coefficient  $\eta$  through the solutions to the Boltzmann equations. In Sect. III, we present our numerical results for a pure pion gas and a pion-nucleon gas mixture. We introduce a criterion which measures the validity region of the calculations. The use of phenomenological cross sections is very important to enlarge the range of validity. We discuss in detail the effects of chemical potential on  $\eta$  and  $\eta/s$  and examine the interpretation of the valley structure as the liquid-gas phase transition. Summary is given in the last section.

## II. KINETIC THEORY OF A HADRONIC GAS MIXTURE

### A. Quantum Boltzmann equations

We first explain our theoretical framework which is necessary for computing the shear viscosity coefficient. Consider a dilute gas of pions ( $\pi$ ) and nucleons ( $N$ ) in which particles interact with each other through binary collisions. Nonequilibrium processes such as relaxation to thermal equilibrium can be described by kinetic equations for one particle distribution functions  $f^\pi(\mathbf{x}, \mathbf{p}, t)$  and  $f^N(\mathbf{x}, \mathbf{p}, t)$  (below, we suppress  $\mathbf{x}$ -dependence). For simplicity, we assume that the gas is isospin symmetric, and thus  $f^\pi(\mathbf{p}, t)$  and  $f^N(\mathbf{p}, t)$  are isospin averaged distributions. The relativistic quantum Boltzmann equations (more precisely, the Uehling-Uhlenbeck equations) of this hadronic gas mixture are then given by

$$\frac{p^\mu}{E_p^\pi} \partial_\mu f^\pi(p) = \mathcal{C}^{\pi\pi} [f^\pi, f^\pi] + \mathcal{C}^{\pi N} [f^\pi, f^N], \quad (1)$$

$$\frac{p^\mu}{E_p^N} \partial_\mu f^N(p) = \mathcal{C}^{NN} [f^N, f^N] + \mathcal{C}^{N\pi} [f^N, f^\pi], \quad (2)$$

where  $E_p^{\pi,N} = \sqrt{m_{\pi,N}^2 + p^2}$  and the collision terms are defined as

$$\begin{aligned}
\mathcal{C}^{\pi\pi} + \mathcal{C}^{\pi N} &= \frac{g_\pi}{2} \int d\Gamma^{\pi\pi} \left\{ f_1^\pi f_2^\pi (1 + f_3^\pi) (1 + f_p^\pi) - (1 + f_1^\pi) (1 + f_2^\pi) f_3^\pi f_p^\pi \right\} \\
&\quad + g_N \int d\Gamma^{\pi N} \left\{ f_1^N f_2^\pi (1 - f_3^N) (1 + f_p^\pi) - (1 - f_1^N) (1 + f_2^\pi) f_3^N f_p^\pi \right\}, \\
\mathcal{C}^{NN} + \mathcal{C}^{N\pi} &= \frac{g_N}{2} \int d\Gamma^{NN} \left\{ f_1^N f_2^N (1 - f_3^N) (1 - f_p^N) - (1 - f_1^N) (1 - f_2^N) f_3^N f_p^N \right\} \\
&\quad + g_\pi \int d\Gamma^{N\pi} \left\{ f_1^\pi f_2^N (1 + f_3^\pi) (1 - f_p^N) - (1 + f_1^\pi) (1 - f_2^N) f_3^\pi f_p^N \right\}.
\end{aligned} \tag{3}$$

We have used shorthand notation  $f_i^{\pi,N} \equiv f^{\pi,N}(k_i)$ ,  $f_p^{\pi,N} \equiv f^{\pi,N}(p)$  and  $g_\pi, g_N$  are the degeneracy factors  $g_\pi = 3$ ,  $g_N = 2$ . For the collisions between the same species ( $\pi\pi$ ,  $NN$ ), we have added a factor  $1/2$ . The factors  $(1 + f^\pi)$  and  $(1 - f^N)$  represent the Bose-Einstein and Fermi statistics of particles, respectively. Finally,  $d\Gamma$  in the integrands are invariant measures with the scattering amplitudes squared: For example,

$$d\Gamma^{\pi N} \equiv |M_{\pi N}|^2 \frac{(2\pi)^4 \delta^{(4)}(k_1 + k_2 - k_3 - p)}{(2E_1^N)(2E_2^\pi)(2E_3^N)(2E_p^\pi)} \prod_i \frac{d^3 k_i}{(2\pi)^3}, \tag{5}$$

where  $M_{\pi N}$  is the elastic scattering amplitude for  $N(k_1) + \pi(k_2) \rightarrow N(k_3) + \pi(p)$ . Explicit form of the scattering amplitudes will be shown at the end of this section. These are the basic ingredients of the kinetic theory.

Before we discuss how to solve the Boltzmann equations (1) and (2), we need to know the equilibrium states. We define them without solving the full Boltzmann equations: They are given by the distributions  $f_0^\pi, f_0^N$  which make the collision terms vanish. Namely,  $\mathcal{C}^{\pi\pi}[f_0^\pi, f_0^\pi] + \mathcal{C}^{\pi N}[f_0^\pi, f_0^N] = \mathcal{C}^{N\pi}[f_0^N, f_0^\pi] + \mathcal{C}^{NN}[f_0^N, f_0^N] = 0$ . These conditions are easily satisfied by the following Bose-Einstein and Fermi-Dirac distributions if the common temperature  $T = 1/\beta$  and hydrodynamic velocity  $V^\mu$  are used

$$f_0^\pi(p) = \frac{1}{e^{\beta V_\mu p^\mu} - 1}, \tag{6}$$

$$f_0^N(p) = \frac{1}{e^{\beta(V_\mu p^\mu - \mu)} + 1}, \tag{7}$$

where  $\mu$  is the baryon chemical potential. The parameters  $T$ ,  $V^\mu$  and  $\mu$  can, in principle, depend on the coordinates (local equilibrium), but when we compute quantities in thermal equilibrium, we simply select the rest frame  $V^\mu = (1, 0, 0, 0)$  so that  $V_\mu p^\mu = E$ .

In evaluating the entropy density, we use the expression in the equilibrium state as is done in the literature because the deviation from the equilibrium is assumed to be small. Namely, by using the grand partition functions

for  $\pi$  and  $N$ ,

$$\ln Z_\pi = -V g_\pi \int \frac{d^3 p}{(2\pi)^3} \ln \left( 1 - e^{-\frac{E^\pi}{T}} \right), \tag{8}$$

$$\ln Z_N = V g_N \int \frac{d^3 p}{(2\pi)^3} \ln \left( 1 + e^{-\frac{E^N - \mu}{T}} \right), \tag{9}$$

one obtains the total entropy density  $s = s_\pi + s_N$  as follows:

$$\begin{aligned}
s_\pi &= \frac{1}{V} \frac{\partial}{\partial T} T \ln Z_\pi \\
&= -g_\pi \int \frac{dp}{2\pi^2} p^2 \left\{ \ln \left( 1 - e^{-\frac{E^\pi}{T}} \right) - \frac{E^\pi}{T(e^{\frac{E^\pi}{T}} - 1)} \right\}, \\
s_N &= \frac{1}{V} \frac{\partial}{\partial T} T \ln Z_N \\
&= g_N \int \frac{dp}{2\pi^2} p^2 \left\{ \ln \left( 1 + e^{-\frac{E^N - \mu}{T}} \right) + \frac{E^N - \mu}{T(e^{\frac{E^N - \mu}{T}} + 1)} \right\}.
\end{aligned}$$

## B. Shear viscosity coefficient

The shear viscosity coefficient is defined through the deviation of spatial components of the energy momentum tensor in the linear order with respect to fluctuation from the equilibrium. Consider a nonequilibrium state which is slightly deviated from the global equilibrium. Small deviation of the space components of energy momentum tensor ( $T^{ij} = T_0^{ij} + \delta T^{ij}$ ) can be divided into traceful and traceless parts:

$$\delta T^{ij} \equiv \zeta (\delta^{ij} \nabla \cdot \mathbf{V}) - 2\eta (\nabla^i V^j)_{\text{trl}}, \tag{10}$$

$$(\nabla^i V^j)_{\text{trl}} \equiv \frac{1}{2} (\nabla^i V^j + \nabla^j V^i) - \frac{\delta^{ij}}{3} \nabla \cdot \mathbf{V}, \tag{11}$$

where  $V^i$  is a space component of the hydrodynamic four velocity (which is common for  $\pi$  and  $N$ )

$$V^\mu = \frac{\int d^3 p \frac{p^\mu}{E^{\pi,N}} f^{\pi,N}(p)}{\int d^3 p f^{\pi,N}(p)}.$$

Eq. (10) is the definition of the shear and bulk viscosity coefficients  $\eta$  and  $\zeta$ . The flow vector  $V^i$ , as well as  $T$

and  $\mu$ , is in principle arbitrary and can depend on spatial coordinates. But below we consider the case where only the flow vector  $V^i$  depends on the coordinates, and in particular, its divergence is vanishing:  $\nabla^i V^i = 0$  and  $\nabla^i V^j \neq 0$  ( $i \neq j$ ). This situation corresponds to considering only the shear viscosity coefficient  $\eta$  and ignoring all the other transport coefficients such as bulk viscosity or heat conductivity.

If one knows distributions  $f^{\pi,N}(p) = f_0^{\pi,N}(p) + \delta f^{\pi,N}(p)$  as the solutions to the Boltzmann equations (1) and (2), one can explicitly compute the (deviation of) energy momentum tensor:

$$\begin{aligned} \delta T^{ij} &= g_\pi \int \frac{d^3 p}{(2\pi)^3} \frac{p^i p^j}{E_p^\pi} \delta f^\pi(p) \\ &+ g_N \int \frac{d^3 p}{(2\pi)^3} \frac{p^i p^j}{E_p^N} \delta f^N(p). \end{aligned} \quad (12)$$

As mentioned above, we consider only the deviation  $\delta f^{\pi,N}$  that originates from the shear. Then, it is quite convenient to parametrize  $\delta f^\pi$  and  $\delta f^N$  as follows ( $\hat{p}_i = p_i/p$ ):

$$\begin{aligned} \delta f^\pi &\equiv -f_0^\pi(1 + f_0^\pi) \beta B^\pi(p) \\ &\times \left( \hat{p}_i \hat{p}_j - \frac{\delta_{ij}}{3} \right) (\nabla^i V^j)_{\text{tr1}}, \end{aligned} \quad (13)$$

$$\begin{aligned} \delta f^N &\equiv -f_0^N(1 - f_0^N) \beta B^N(p) \\ &\times \left( \hat{p}_i \hat{p}_j - \frac{\delta_{ij}}{3} \right) (\nabla^i V^j)_{\text{tr1}}, \end{aligned} \quad (14)$$

where we have introduced new quantities  $B^{\pi,N}(p)$  to be determined by the Boltzmann equations.

Substituting Eqs. (13) and (14) into Eq. (12) and comparing the result with Eq. (10), one finds the shear viscosity coefficient  $\eta$  as a function of unknown functions  $B^{\pi,N}(p)$ :

$$\begin{aligned} \eta &= \frac{g_\pi \beta}{15} \int \frac{d^3 p}{(2\pi)^3} \frac{f_0^\pi(1 + f_0^\pi)}{E_p^\pi} p^2 B^\pi(p) \\ &+ \frac{g_N \beta}{15} \int \frac{d^3 p}{(2\pi)^3} \frac{f_0^N(1 - f_0^N)}{E_p^N} p^2 B^N(p). \end{aligned} \quad (15)$$

The unknown functions  $B^{\pi,N}(p)$  (or equivalently, the deviations  $\delta f^{\pi,N}$ ) are numerically determined by solving the Boltzmann equations that are linearized with respect to  $\delta f^{\pi,N}$ . This procedure corresponds to the lowest order Chapman-Enskog method. Here we discuss only the outline of the procedure to solve the Boltzmann equations. More details are discussed in Appendix B.

After the linearization, the Boltzmann equations (1), (2) become a coupled linear equations for  $B^\pi(p)$  and  $B^N(p)$ . Following Ref. [12], we solve these equations in the functional space spanned by the orthogonal polynomials  $\{W_{(n)}(p), n = 0, 1, 2, \dots\}$ . Let us expand  $B^{\pi,N}(p)$  by these bases:

$$B^{\pi,N}(p) = \sum_{n=0}^{\infty} b_{(n)}^{\pi,N} W_{(n)}^{\pi,N}(p), \quad (16)$$

where  $W_{(n)}^{\pi,N}(p)$  is a polynomial of the order  $n$ , and  $b_{(n)}^{\pi,N}$  is the coefficient independent of  $p$ . Notice that  $W_{(n)}^\pi(p)$  and  $W_{(n)}^N(p)$  are not equivalent to each other. Indeed, they are defined so that they satisfy the following different orthogonal conditions:

$$\int \frac{d^3 p}{(2\pi)^3} \frac{f_0^\pi(1 + f_0^\pi)}{E_p^\pi} p^2 W_{(n)}^\pi(p) W_{(m)}^\pi(p) = \delta_{nm} L_{(n)}^\pi, \quad (17)$$

$$\int \frac{d^3 p}{(2\pi)^3} \frac{f_0^N(1 - f_0^N)}{E_p^N} p^2 W_{(n)}^N(p) W_{(m)}^N(p) = \delta_{nm} L_{(n)}^N. \quad (18)$$

The normalization factors  $L_{(n)}^\pi$  and  $L_{(n)}^N$  are not chosen to be 1. Instead, we choose the polynomial so that the coefficient of the term with the highest degree is unity (such polynomials are called "monic"). Namely, the first three polynomials have the following form:

$$\begin{aligned} W_{(0)}(p) &= 1, \\ W_{(1)}(p) &= p + c_1, \\ W_{(2)}(p) &= p^2 + d_1 p + d_2. \end{aligned}$$

Parameters  $c_1$ ,  $d_1$  and  $d_2$  are uniquely determined by the orthogonal conditions (thus independent of the dynamics). In fact,  $W_{(n)}$  has  $n$  unknown parameters, which are uniquely determined by  $n$  orthogonal conditions with lower polynomials ( $W_{(m)}$ ,  $m = 0, \dots, n-1$ ). Thus,  $L_{(n)}^\pi$  and  $L_{(n)}^N$  in Eqs. (17) and (18) are known after we completely determine  $W_{(n)}$ . Practically, the expansion (16) is well approximated by the first few terms. Thus, in the present analysis, we take only the first three terms:

$$B^\pi(p) \simeq b_{(0)}^\pi + b_{(1)}^\pi W_{(1)}^\pi(p) + b_{(2)}^\pi W_{(2)}^\pi(p), \quad (19)$$

$$B^N(p) \simeq b_{(0)}^N + b_{(1)}^N W_{(1)}^N(p) + b_{(2)}^N W_{(2)}^N(p), \quad (20)$$

where we have used the definition  $W_{(0)}^{\pi,N} = 1$ . The coefficients  $b_{(n)}^{\pi,N}$  are numerically determined. Once we know these coefficients, we can compute the shear viscosity coefficient  $\eta$  from Eq. (15). We have checked that the results do not change even if we take up to the fourth terms ( $n \leq 3$ ).

Two comments are in order about our formulation. Firstly, we recall that the expansion of  $B^{\pi,N}(p)$  in Eq. (16) is a familiar technique in solving the Boltzmann equation by the Chapman-Enskog method. If one treated a *classical* Boltzmann equation, measure of the orthogonal condition would be given by a much simpler distribution, the Maxwell-Boltzmann distribution. In this case, the polynomials that satisfy the orthogonal condition are given by famous functions, the Sonine polynomials [19]. For the *quantum* Boltzmann equation, however, the measure in the orthogonal condition is given by either the Fermi-Dirac or Bose-Einstein distribution, as shown in Eqs. (17) and (18). In this case, the polynomials satisfying them are not known, and we have to find them order by order.

Secondly, note that the shear viscosity coefficient  $\eta$  defined by Eq. (15) may be formally written as

$$\eta = \eta^\pi + \eta^N. \quad (21)$$

It apparently looks ‘additive’ with respect to each contribution. Indeed, if one considers a pion gas system without nucleons, one finds exactly the same expression as the first term of Eq. (15). One might then be tempted to conclude from the expression (21) that the inclusion of nucleons always contributes to enhance the value of shear viscosity. However, such argument does not make sense because the function  $B^\pi(p)$  itself will change by the inclusion of nucleons. We will see later that  $\eta^\pi$  indeed *decreases* as the effects of nucleons become large (i.e., with increasing chemical potential).

### C. Scattering amplitudes of binary collisions

Let us show the explicit expression of the scattering amplitudes in the collision terms (3), (4), and (5). Note that we have assumed factorization of the scattering amplitudes from the products of one-particle distributions in the collision terms. This is physically natural in a dilute gas where each collision is simply treated as an independent binary collision (ignoring higher order multiparticle correlations). Therefore, as long as we consider a dilute gas system where the Boltzmann equation is applicable, it is reasonable to use the amplitudes for two particle scatterings in the vacuum (free space). This is a great merit in computing transport coefficients. If one follows the microscopic Kubo formula to compute the transport coefficients, it is quite nontrivial how to include the effects of physical processes. On the other hand, if one uses the Boltzmann equation, one can easily incorporate the physical cross sections in the collision terms, which is however less justified from the first principle. In the present paper, we examine two different parametrizations for the scattering amplitudes. One is based on theoretical calculations, while the other is constructed from the experimental data. More precisely, we use the amplitudes from the low energy effective field theory (EFT) on the one hand, and the phenomenological amplitudes designed to reproduce experimental data of the elastic scatterings on the other hand.

Scattering amplitudes based on EFT are the following. First of all, the isospin-averaged  $\pi\pi$  scattering amplitude is given by the leading order Chiral Perturbation Theory (LO-ChPT) [20]:

$$|M_{\pi\pi}|^2 = \frac{1}{9f_\pi^4} \left\{ 21m_\pi^4 + 9s^2 - 24m_\pi^2s + 3(t-u)^2 \right\}, \quad (22)$$

where  $f_\pi$  is the pion decay constant ( $f_\pi = 93$  MeV),  $s$ ,  $t$  and  $u$  are the Mandelstam variables for the scattering  $\pi(k_1) + \pi(k_2) \rightarrow \pi(k_3) + \pi(p)$ .

Next, for the  $\pi N$  scattering, we use the results of low energy effective theory (LO heavy baryon ChPT) [21].

The isospin averaged  $\pi N$  scattering amplitude in the Center-of-Mass (CM) frame is

$$|M_{\pi N}|^2 = (2m_N)^2 \left\{ 4|g_-|^2 + 2q_{\text{cm}}^4 \sin^2 \theta_{\text{cm}} |h_+|^2 \right\}, \quad (23)$$

where  $q_{\text{cm}}$  and  $\theta_{\text{cm}}$  are, respectively, the magnitude of pion momentum, and the scattering angle in the CM frame. Two functions  $g_-$  and  $h_+$  are

$$g_- = -\frac{g_A^2}{f_\pi^2} \frac{1}{4\omega} (2\omega^2 - 2m_\pi^2 + t) + \frac{\omega}{2f_\pi^2},$$

$$h_+ = -\frac{g_A^2}{f_\pi^2} \frac{1}{2\omega},$$

where  $g_A = 1.26$  is the nucleon axial charge, and  $\omega$  is the pion energy in the CM frame. Note that the overall factor in Eq. (23) is not the same as in Ref. [16] though both are based on Ref. [21]. This is because we have used the standard normalization factor for the spinors  $\bar{u}^r(p)u^s(p) = 2m_N\delta^{rs}$  instead of  $\bar{u}^r(p)u^s(p) = \{(E^N + m_N)/2m_N\}\delta^{rs}$  which was adopted in Ref. [21].

Lastly, let us consider the  $NN$  scattering. In the low energy EFT, scattering amplitudes in the CM frame for fixed spin and isospin can be parametrized in terms of the scattering length  $a$  and the effective range  $r$  as

$$|M_{NN'}|^2 = 64\pi^2 \mathbf{s} \cdot \frac{1}{|-a^{-1} + \frac{1}{2}r q_{\text{cm}}^2 - i q_{\text{cm}}|^2}, \quad (24)$$

where  $q_{\text{cm}}$  is the magnitude of nucleon momentum in the CM frame. For each process, parameters  $a$  and  $r$  are determined to fit the low energy experimental data with the contribution from Coulomb force removed. Their numerical values are shown in table I. They are taken from Ref. [22]:

TABLE I: Scattering length  $a$  and effective range  $r$  for  $NN$  collisions.

system	parameter	$S = 0, I = 1$	$S = 1, I = 0$
$pp$	$a$	-17.1 (fm)	—
	$r$	2.79 (fm)	—
$nn$	$a$	-16.6 (fm)	—
	$r$	2.84 (fm)	—
$np$	$a$	-23.7 (fm)	5.42 (fm)
	$r$	2.73 (fm)	1.73 (fm)

In low energy scattering, the dominant contribution to the amplitude is given by the  $s$ -wave (orbital angular momentum  $\ell = 0$ ). Thus, we construct the spin-isospin averaged scattering amplitude from the expression (24) for the  $s$ -wave with appropriate weight factors of spin and isospin. Details of the spin-isospin average are explained in Appendix A.

In summary, the scattering amplitudes based on EFT are given by Eqs. (22), (23), and (24). It should be emphasized that all these expressions of the scattering amplitudes are valid only in a limited region of kinematics. LO-ChPT (for  $\pi\pi$  case) is usually considered to be

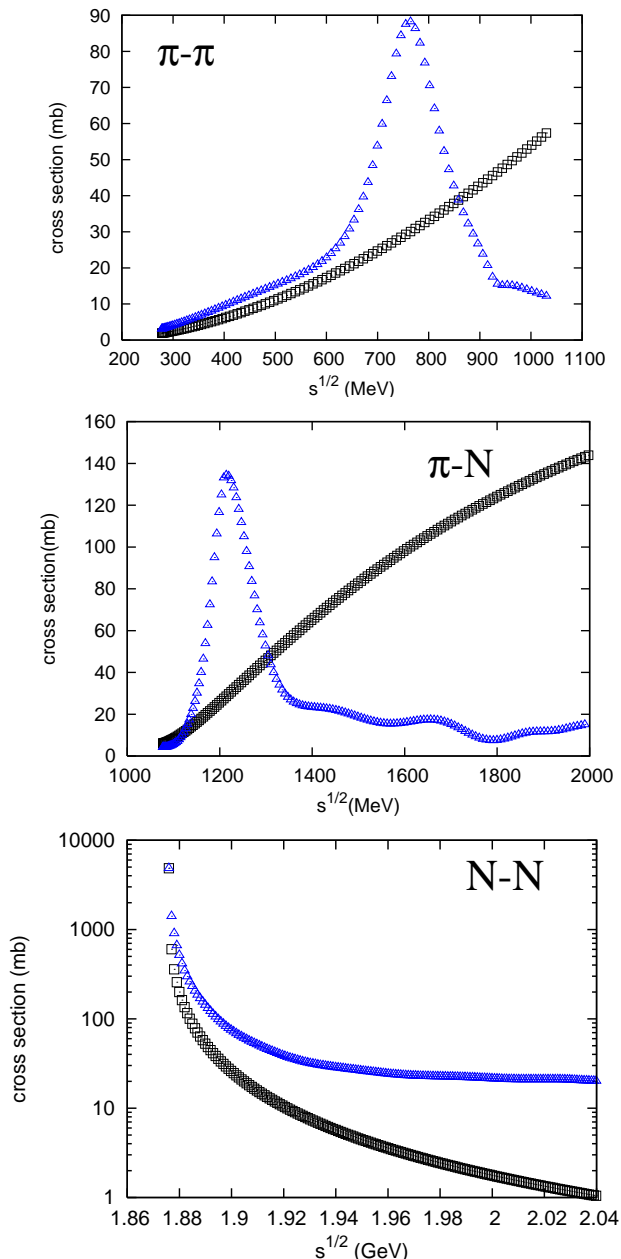


FIG. 1: (Color online) Comparison of the elastic cross sections in  $\pi\pi$ ,  $\pi N$ , and  $NN$  scatterings. Square and triangle points are the results of the low energy EFT and the phenomenological amplitudes, respectively. The actual fit to the experimental data was done for the differential cross sections. The  $NN$  elastic cross section is shown in logarithmic scale.

valid for  $p \ll 4\pi f_\pi \sim 1$  GeV with  $p$  being the magnitude of pion momentum. In the heavy baryon ChPT for the  $\pi N$  case, there is an additional expansion parameter  $p/m_N \ll 1$ , which gives almost the same limitation as for the  $\pi\pi$  case. Lastly, for the  $NN$  case, the differential cross section (24) is valid only for small  $q_{\text{cm}}$ , or equivalently, small scattering energy near the threshold. This fact implies that the validity of results derived from the

Boltzmann equations will also be restricted to a small region in the  $T$ - $\mu$  plane, as we will discuss later.

With this limitation in mind, it is quite important to consider physical scattering amplitudes in order to check the usefulness of, or more importantly to go beyond, the low energy EFT. To this end, we have constructed *phenomenological amplitudes* from the experimental data (differential cross sections) by fitting the coefficients of the partial-wave expansion. The fit was performed to the data up to  $\sqrt{s} = 1.15$  GeV ( $q_{\text{cm}} = 550$  MeV) in the  $\pi\pi$  scattering,  $\sqrt{s} = 2.00$  GeV ( $q_{\text{cm}} = 770$  MeV) in the  $\pi N$  scattering, and  $\sqrt{s} = 2.04$  GeV ( $q_{\text{cm}} = 405$  MeV) in the  $NN$  scattering. Details of the fitting procedure are discussed in Appendix A. In Fig. 1, we compare elastic cross sections of the two different parametrizations. The elastic cross sections from the phenomenological amplitudes are almost identical with the experimental data (not shown) in the energy regions shown in the figures. Peaks in  $\pi\pi$  and  $\pi N$  cross sections are  $\rho$ -meson and  $\Delta$  resonances, respectively. As mentioned above, the range of validity of LO-ChPT (for  $\pi\pi$ ,  $\pi N$  cases) is  $p \ll 1$  GeV for the pion momentum. Thus, if one applies this limitation to the momentum of colliding particles in the CM frame, one finds for the scattering energy  $\sqrt{s} \ll \sqrt{s_0}$  with  $\sqrt{s_0} \sim 2$  GeV for the  $\pi\pi$  scattering, and  $\sqrt{s_0} \sim 2.4$  GeV for the  $\pi N$  scattering. Indeed, as evident from the figure, deviation of LO-ChPT from the phenomenological cross sections is already sizable well below the upper limits (mainly because of the  $\rho$ -meson and  $\Delta$  resonances). For example, in the  $\pi\pi$  case, LO-ChPT gives the same tendency as the phenomenological cross section up to  $\sqrt{s} \sim 600$  MeV ( $q_{\text{cm}} \sim 270$  MeV), but beyond that the deviation is not small. Therefore, it would be safe to consider the validity region of LO-ChPT to be

$$\sqrt{s} \lesssim \sqrt{s_{\text{max}}^{\text{EFT}}} \equiv 600 \text{ MeV} \quad (\pi\pi \text{ scattering}), \quad (25)$$

which is of course within  $\sqrt{s} \ll \sqrt{s_0} \sim 2$  GeV. Later we will use this limit to evaluate the maximum temperature up to which LO-ChPT is applicable. From the figures, it is obvious that the difference of two parametrizations becomes larger and larger with increasing energies. The  $\pi\pi$  and  $\pi N$  cross sections from LO-ChPT monotonically increase and become too large compared to the actual physical cross sections. We will see in the next section that this difference greatly affects the numerical value of the shear viscosity.

### III. NUMERICAL RESULTS

#### A. Pion gas

Let us first discuss the case with only pions. This is important for properly understanding the effects of nucleons in the next subsection and, at the same time, for checking the validity of our calculation compared with the existing results [14, 15]. As we mentioned before, our

formalism for the  $\pi N$  gas can be easily reduced to the case with only pions (by setting the nucleon degeneracy factor  $g_N \rightarrow 0$ , for example). Then, the shear viscosity coefficient is given by the first term of Eq. (15), and we determine  $B^\pi(p)$  by solving the Boltzmann equation (1) with the collision term given by the first term of Eq. (3). The expansion of  $B^\pi(p)$  with respect to the orthogonal polynomials was taken up to the third order to ensure the convergence of the result.

### 1. Range of validity

Before presenting our numerical results, we clarify the range of validity in temperature for two parametrizations of the scattering amplitudes. As we already specified in Eq. (25), LO-ChPT is valid only in a limited kinematical regime:  $\sqrt{s} \lesssim \sqrt{s_{\max}^{\text{EFT}}} = 600$  MeV, while the phenomenological amplitude is by construction valid up to  $\sqrt{s} = 1.15$  GeV. These conditions can be translated to the limitation in temperature in the following way. Consider the binary collisions in thermal equilibrium. Since each collision takes place between particles in thermal equilibrium, the scattering energy squared  $s$  will fluctuate around its mean value  $\langle s \rangle$  with a width  $\Sigma$ . The average  $\langle s \rangle$  and the width (standard deviation)  $\Sigma$  may be defined by

$$\langle s \rangle \equiv \frac{\int \frac{d^3 p_1}{(2\pi)^3} \int \frac{d^3 p_2}{(2\pi)^3} s(p_1, p_2) f_0^\pi(p_1) f_0^\pi(p_2)}{\int \frac{d^3 p_1}{(2\pi)^3} \int \frac{d^3 p_2}{(2\pi)^3} f_0^\pi(p_1) f_0^\pi(p_2)}, \quad (26)$$

$$\Sigma \equiv \sqrt{\langle s^2 \rangle - \langle s \rangle^2}. \quad (27)$$

Because the scattering energy squared of most of the collisions are below  $s_{\max}(T) \equiv \langle s \rangle + \Sigma$ , one can regard  $s_{\max}(T)$  as (a measure of) the highest energy squared at temperature  $T$ . So, one may interpret the validity condition of LO-ChPT as  $s_{\max}(T) < s_{\max}^{\text{EFT}} = 0.36$  GeV<sup>2</sup>, and thus obtain the validity condition for temperature  $T < T_{\max}^{\text{EFT}}$  with  $T_{\max}^{\text{EFT}}$  given by  $s_{\max}(T_{\max}^{\text{EFT}}) = 0.36$  GeV<sup>2</sup>. In Fig. 2, we show  $\langle s \rangle$  and  $s_{\max}$  as functions of temperature. From the figure, one can read  $T_{\max}^{\text{EFT}} \sim 70$  MeV. Therefore, we may conclude that the results of LO-ChPT are reliable only up to  $T \sim 70$  MeV. On the other hand, the phenomenological amplitude is valid up to  $s \sim 1.3$  GeV<sup>2</sup>. Therefore, we expect from the figure that the results of the phenomenological amplitude will be reliable up to temperature close to  $T_c \sim 170$  MeV.

There is another important check for the validity of our framework. It is the applicability of the Boltzmann equations. Recall that in deriving the Boltzmann equations, one assumes that a two-point correlation function can be factorized into a product of two one-point functions (one particle distributions  $f(x, p, t)$ ). This is physically acceptable when the density of particles  $n$  is small enough. This condition is normally expressed as

$$\lambda \gg d \quad (28)$$

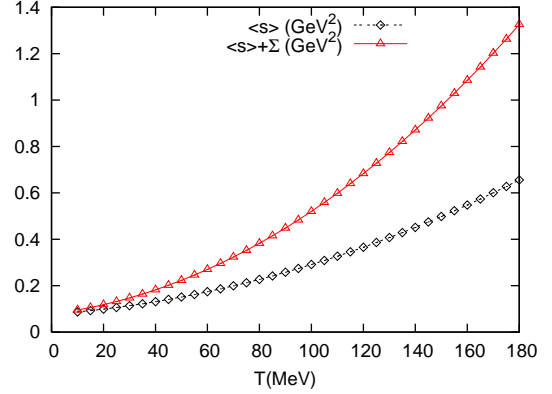


FIG. 2: (Color online) Temperature dependence of the average scattering energy squared ( $s$ ) and the measure of highest scattering energy squared  $s_{\max} = \langle s \rangle + \Sigma$ .

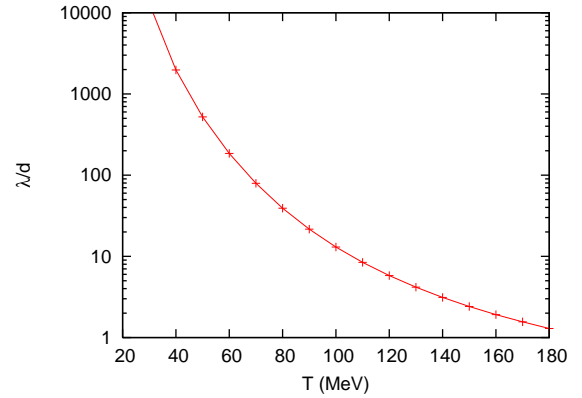


FIG. 3: (Color online) The ratio  $\lambda/d$  as a function of temperature  $T$ . The description based on the Boltzmann equation is valid when  $\lambda/d \gg 1$ .

where  $\lambda$  is the mean-free path

$$\lambda = \frac{1}{n\sigma} \quad (29)$$

with  $\sigma$  being the cross section, and  $d$  is the interaction range, meaning that each collision takes place independently. If we define the interaction range  $d$  by the Compton length of pions:  $d \sim 1/m_\pi$ , then the validity condition for the Boltzmann equation reads  $\lambda/d \sim m_\pi/n\sigma \gg 1$ . Alternatively, if we define  $d$  through the cross section as  $\sigma \sim \pi d^2$ , we obtain another expression  $\lambda/d \sim \sqrt{\pi/\sigma^3}/n \gg 1$ . Both expressions give similar restriction on temperature. Figure 3 shows the ratio  $\lambda/d$  as a function of temperature, where the (phenomenological) cross section  $\sigma$  is estimated by its thermal average. One finds  $\lambda/d \gtrsim 3$  at  $T = 140$  MeV, which manages to satisfy the inequalities. At this temperature, the mean-free path of pions is estimated as  $\lambda \sim 4$  fm, which is consistent with the literature [23]. As the temperature is decreased, the mean-free path becomes longer, and the Boltzmann description gets better and better.



Combining these two results, we may conclude that the phenomenological analysis of a pion gas based on the Boltzmann equation will be valid up to temperature  $T \sim 140$  MeV which is much higher than the LO-ChPT limit  $T \sim 70$  MeV, but lower than the critical temperature  $T_c \sim 170$  MeV. However, we notice that there is a caveat to this conclusion. In fact, even though we have satisfactory description of  $\pi\pi$  scatterings in wider kinematical regime, we have to worry about at least two other effects as temperature increases. The first one is the effects of other (heavier) degrees of freedom such as kaons, and the second is the possible modification of pions in thermal environment. Both are however beyond the scope of the paper and we leave them for future problems.

## 2. Shear viscosity coefficient $\eta$

Figure 4 shows the shear viscosity coefficient  $\eta$  as a function of temperature  $T$ . Open diamonds ( $\diamond$ ) and open triangles ( $\triangle$ ) are based on numerical solutions to the Boltzmann equations with the phenomenological amplitudes and LO-ChPT, respectively. Remarkably, the two results show quite different behavior. While the result of LO-ChPT decreases with increasing  $T$ , that of the phenomenological amplitude shows the opposite behavior.

Qualitative behavior of two different results can be easily understood by using rough estimate of the viscosity coefficient. In classical transport theory for a dilute gas of one component, the shear viscosity coefficient is expressed in terms of the mean-free path  $\lambda = 1/n\sigma$ , Eq. (29), as follows:

$$\eta \sim \frac{1}{3}n\bar{p}\lambda, \quad (30)$$

where  $n$  is the particle number density,  $\bar{p}$  is the average momentum, and  $\sigma$  is the binary cross section. Thus, the shear viscosity coefficient is inversely proportional to the cross section. As we already saw in Fig. 2, the typical energy in the  $\pi\pi$  scattering increases with temperature. This means that average cross section  $\langle\sigma\rangle$  indirectly depends on temperature. Notice also that the average momentum  $\bar{p} = \int d^3p |\mathbf{p}| f_0^\pi(p) / \int d^3p f_0^\pi(p)$  roughly increases like  $\bar{p} \propto \sqrt{T}$  (because  $(\bar{p})^2/2m \sim 3kT/2$ ). Therefore, temperature dependence of the shear viscosity coefficient is essentially determined by the interplay between those of  $\bar{p}$  and  $\langle\sigma\rangle$ . For example, if the average cross section  $\langle\sigma\rangle$  increases rapidly as a function of  $T$  (faster than  $\sqrt{T}$ ),  $\eta \sim \bar{p}/\langle\sigma\rangle$  is a decreasing function of  $T$ . But if  $\langle\sigma\rangle$  is almost constant,  $\eta$  is an increasing function of  $T$ . Based on these considerations and Fig. 1, we can easily deduce the followings: As for the temperature dependence of the shear viscosity, we expect that  $\eta_{\text{pheno}}$  is slightly smaller than  $\eta_{\text{ChPT}}$  at low temperature (because  $\sigma_{\text{pheno}} \gtrsim \sigma_{\text{ChPT}}$ ), while  $\eta_{\text{pheno}} > \eta_{\text{ChPT}}$  at high temperature. More precisely, since  $\langle\sigma\rangle$  of the ChPT monotonically increases as  $\langle\sigma\rangle \sim T^2/f_\pi^4$  while that of the phe-

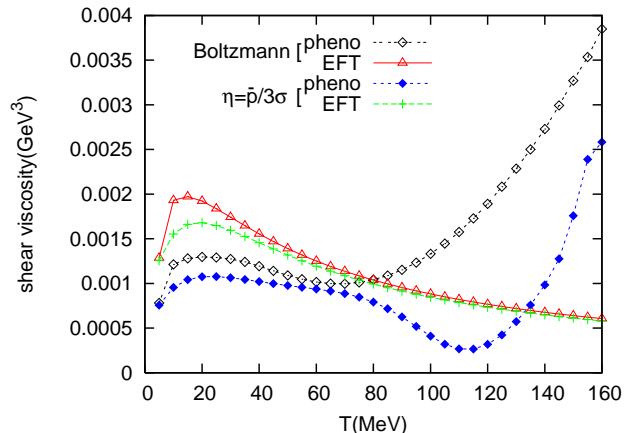


FIG. 4: (Color online) Shear viscosity coefficient  $\eta$  of a pion gas as a function of temperature. Numerical results from the Boltzmann equations are compared with the rough estimate (30).

nomenological amplitude does not grow, we expect that the shear viscosity decreases in the ChPT case while the opposite happens in the phenomenological case.

Now let us come back to Fig. 4, where we also show the rough estimate (30) with two different parametrizations. For the (average) cross section  $\sigma$  in the rough estimate (30), we evaluate it at the average momentum  $\bar{p}$ , i.e.,  $\langle\sigma\rangle \equiv \sigma(\bar{p}(T))$ . [32] Comparing the results of the Boltzmann equations and of the rough estimate (30), we find that qualitative agreement of the results in two different ways of computation. Nontrivial behavior of the rough estimate for the phenomenological amplitude (filled diamond points) is due to the resonance shape of the elastic cross section in Fig. 1. Indeed, the valley around  $T \sim 110$  MeV corresponds to the  $\rho$  meson peak around  $s \sim 0.5$  GeV<sup>2</sup> in the  $\pi\pi$  cross section (According to Fig. 2,  $s \sim 0.5$  GeV<sup>2</sup> is translated into  $T \sim 150$  MeV, which is further diminished due to  $\bar{p} \sim \sqrt{T}$  in the numerator of  $\eta$ ). In the Boltzmann equations, such structure is further washed out by thermal average. From these analyses, we now understand that the behavior of the numerical results of the Boltzmann equations is largely due to the energy dependence of the cross sections used in the collision terms. In particular, the decreasing  $\eta$  of LO-ChPT at relatively high temperature  $T \gtrsim 80$  MeV is an artifact of too large cross section outside of the validity region of LO-ChPT. On the other hand, our most reliable result (open diamonds  $\diamond$  in Fig. 4) shows linear increase with temperature for  $T > 120$  MeV. This behavior is consistent with that of hadronic resonance gas models [9, 24]. Moreover, our result is also consistent with that of Ultrarelativistic Quantum Molecular Dynamics (UrQMD) for a meson gas [17], which also gives linear dependence on  $T$ , and  $\eta \sim 0.1$  GeV·fm<sup>-2</sup> = 0.0039 GeV<sup>-3</sup> at  $T = 150 - 160$  MeV.



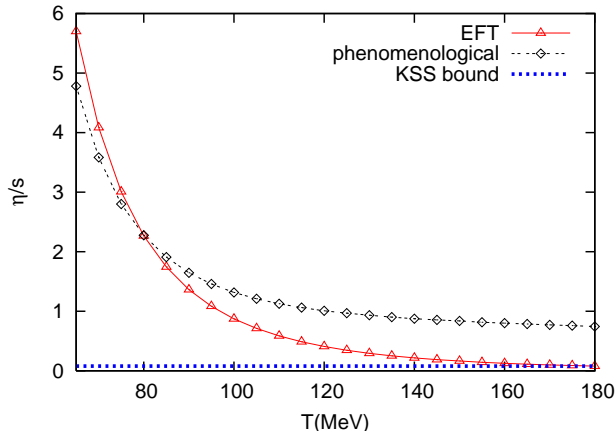


FIG. 5: (Color online) The ratio  $\eta/s$  as a function of temperature  $T$  in a pion gas system. Solid ( $\triangle$ ) and dashed ( $\diamond$ ) curves are, respectively, the results with LO-ChPT and the phenomenological amplitude. Dotted line corresponds to the conjectured lower bound  $\eta/s = 1/4\pi$ .

### 3. The ratio $\eta/s$

Figure 5 shows our numerical results of the ratio  $\eta/s$  as a function of temperature  $T$ . Dashed and solid lines correspond to the results of LO-ChPT and the phenomenological amplitude, respectively. In both cases,  $\eta/s$  is a monotonically decreasing function of  $T$ . Notice that the result of LO-ChPT violates the conjectured bound  $1/4\pi$  (the KSS bound, shown as the dotted line) at around the critical temperature  $T_c \sim 170$  MeV. On the other hand,  $\eta/s$  from the phenomenological amplitude keeps well above the KSS bound up to temperature  $\sim T_c$ . These are consistent with the results of Refs. [14, 15].

Since the entropy density is common in both cases  $s \propto T^3$ , behavior of  $\eta/s$  can be understood by that of  $\eta$  itself. For example, we saw that  $\eta$  decreases in LO-ChPT, while it increases in the phenomenological case. Such difference affects on the ratio  $\eta/s$ : it decreases faster in the LO-ChPT case than in the phenomenological one. Also there is a crossing point for the two results of  $\eta/s$  at  $T \sim 80$  MeV (see Fig. 5), and this point coincides with that of the shear viscosity  $\eta$  (see the open diamonds and open triangles in Fig. 4).

It has been argued in Ref. [14] that violation of the KSS bound  $\eta/s \geq 1/4\pi$  suggests the existence of phase transition (or crossover transition) in order for the KSS bound to remain valid. This kind of argument is of course dangerous because the precise value of  $\eta/s$  depends on the amplitude in the collision term, and the result of Ref. [14] is based on LO-ChPT, whose applicability is limited to  $T \lesssim 70$  MeV as we already discussed in detail. In fact, more reliable result with the phenomenological amplitude does not violate the KSS bound even around the critical temperature. Therefore, “violation of the KSS bound” cannot be the signature of phase transition. Instead of seeing violation of the KSS bound, we propose to check

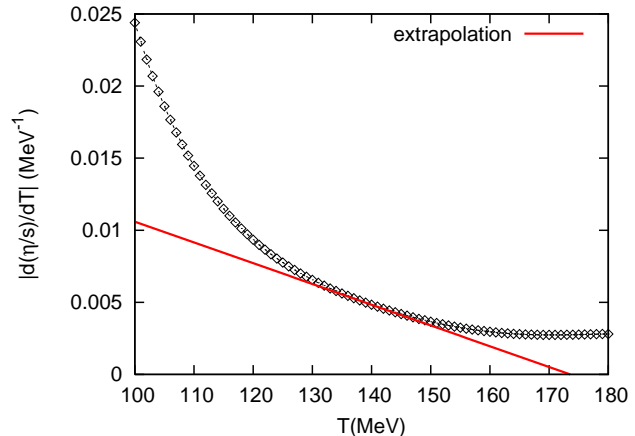


FIG. 6: (Color online) The absolute value of the slope  $|d(\eta/s)/dT|$  for the result of phenomenological amplitude. Straight line is the linear extrapolation at  $T = 140$  MeV.

the other property to catch the indication of phase transition. As we mentioned in Introduction, Ref. [6] suggests that the ratio has a minimum around the (pseudo-) critical temperature  $T_c$ . If this is indeed the case, it implies that (for crossover transition) the curve of  $\eta/s$  as a function of temperature will have a convex form around  $T_c$ , and the slope will decrease as temperature approaches  $T_c$  from the left. (This kind of argument will hold as far as the temperature is not too far away from the critical end point.) What we observed in Fig. 5 for the phenomenological amplitude is indeed the decrease of the slope with increasing temperature. Thus, even if the ratio is still well above the conjectured bound, we can anticipate the existence of phase transition.

In Fig. 6, we show the (absolute value of) slope of the ratio  $\eta/s$  for the phenomenological amplitude. Recall that we have estimated the border of validity region of our calculation to be  $T \sim 140$  MeV. Thus, we use the results around  $T \sim 140$  MeV for linear extrapolation towards higher temperature. More precisely, we approximate the curve  $\mathcal{R}(T) \equiv \eta/s$  around at some temperature  $T = T_0 < T_c$  as

$$\mathcal{R}(T) \simeq \mathcal{R}(T_0) + \mathcal{R}'(T_0)(T - T_0) + \frac{\mathcal{R}''(T_0)}{2}(T - T_0)^2. \quad (31)$$

Then the slope  $d\mathcal{R}(T)/dT$  is approximated by a linear function of  $T$ . The critical temperature  $T_c$  may be defined by the temperature where the slope is zero:  $d\mathcal{R}(T)/dT = 0$ . Namely,

$$T_c \simeq T_0 - \frac{\mathcal{R}'(T_0)}{\mathcal{R}''(T_0)}, \quad (32)$$

where  $\mathcal{R}'(T_0) < 0$  and  $\mathcal{R}''(T_0) > 0$  on the left-hand side of a convex function  $\mathcal{R}(T)$ . The result of linear extrapolation at  $T = T_0 = 140$  MeV is shown on the same figure. Remarkably, the temperature at which the straight line cuts the horizontal axis is 173 MeV, which is quite a reasonable result as the critical temperature. In addition to

this, one can guess the value of  $\eta/s$  at  $T = T_c$  by using the approximation (31):

$$\mathcal{R}(T_c) \simeq \mathcal{R}(T_0) - \frac{(\mathcal{R}'(T_0))^2}{2\mathcal{R}''(T_0)}. \quad (33)$$

If one substitutes numerical values at  $T_0 = 140$  MeV, namely,  $\mathcal{R}(T_0) \simeq 1.0$ ,  $\mathcal{R}'(T_0) \simeq -0.005$  MeV $^{-1}$  and  $\mathcal{R}''(T_0) \simeq 1.38 \times 10^{-4}$  MeV $^{-2}$  which are read from Figs. 5 and 6, one finds  $\mathcal{R} = \eta/s \simeq 0.9$  at  $T = T_c$ . These results should be understood with reservation at least for two reasons. First of all, there is ambiguity in the choice of  $T_0$ , which will affect the values of  $T_c$  and  $\eta/s$ . However, in fact,  $T_0$  cannot be taken arbitrary because we need to take  $T_0$  as close to  $T_c$  as possible for the linear extrapolation to be accurate. To obtain reasonable values of  $T_c$  and  $\eta/s$ , the largest possible value for  $T_0$  is preferable. Since the choice  $T_0 = 140$  MeV is the upper limit of our validity region, we expect that the estimated value  $T_c = 173$  MeV is the best value of our calculation. Therefore, even if there might be some ambiguity in selecting  $T_0$ , we can say that we have chosen the best value. The second source which might change the values of  $T_c$  and  $\eta/s$  is the possible contributions from heavier mesons. Since such contributions become more important as  $T \rightarrow T_c$ , our results with only pions become better as we depart from  $T_c$  (which is however not desirable for determination of  $T_c$ ). Still, we expect our results are not so bad because at  $T \sim 100$  MeV such heavier particles can be ignored, and even at  $T = 140$  MeV, number of kaons amounts to only 20% of total particles.

For the crossover transition, the ratio  $\eta/s$  will be continuous at the (pseudo) critical temperature  $T_c$ . This immediately implies that the numerical value of  $\eta/s$  determined above is relevant even in the deconfined phase. Our result  $\eta/s \sim 0.9$  is well above the KSS bound, but is small enough compared to the weak-coupling QCD result (see for example, Fig. 4 of Ref. [6]). In this sense, the QCD matter around  $T_c$  could be “strongly interacting”. However, we should be careful when we draw such a conclusion from the value of  $\eta/s$ . In fact, the smallness of the ratio  $\eta/s$  is not a direct consequence of large cross section which may be realized by a strongly interacting matter. In our calculation with the phenomenological amplitude, the cross section does not grow a lot (in contrast with the LO-ChPT) and the viscosity  $\eta$  even *increases* as  $T \rightarrow T_c$ . Still, since the entropy increases faster than  $\eta$ , the ratio  $\eta/s$  becomes a decreasing function of temperature. Therefore, the smallness of the ratio is realized in a nontrivial way.

## B. Pion-nucleon gas

Let us now present the numerical results for a dilute  $\pi N$  gas. As advocated in Introduction, addition of nucleons to a pion gas enables us to study the effects of baryon chemical potential. We discuss how the results of

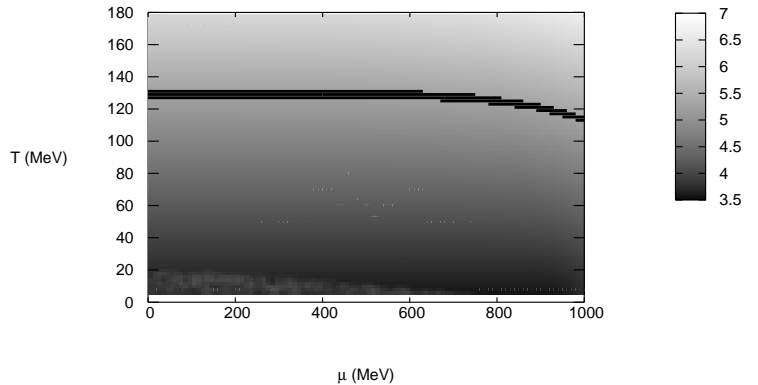


FIG. 7: A measure of the highest scattering energy squared  $\mathfrak{s}_{\max}^{NN} = \langle \mathfrak{s}^{NN} \rangle + \Sigma^{NN}$  for the  $NN$  scattering is plotted in the  $T$ - $\mu$  plane. Gradation represents the values in the range  $3.5 \text{ GeV}^2 < \mathfrak{s}_{\max}^{NN} < 7 \text{ GeV}^2$ . Solid curve corresponds to the borderline  $\mathfrak{s}_{\max}^{NN} = 5.29 \text{ GeV}^2$ .

a pion gas presented in the previous subsection change under the influence of the chemical potential.

### 1. Range of validity

We start again by the discussion on the range of validity of our framework. Since we have to take the  $\pi N$  and  $NN$  collisions into account in the  $\pi N$  gas, we introduce the average scattering energy squared between particles  $i$  and  $j$  ( $i, j = \pi$  or  $N$ ):

$$\langle \mathfrak{s}^{ij} \rangle \equiv \frac{\int \frac{dp_1^3}{(2\pi)^3} \int \frac{dp_2^3}{(2\pi)^3} \mathfrak{s}^{ij}(p_1, p_2) f_0^i(p_1) f_0^j(p_2)}{\int \frac{dp_1^3}{(2\pi)^3} \int \frac{dp_2^3}{(2\pi)^3} f_0^i(p_1) f_0^j(p_2)}. \quad (34)$$

For the  $\pi\pi$  scattering, this is of course equivalent to Eq. (26) and depends only on  $T$ . But for the  $\pi N$  and  $NN$  scatterings, the average values depend on both  $T$  and  $\mu$ . Similarly as before, we further define the standard deviation by  $\Sigma^{ij} \equiv \sqrt{\langle (\mathfrak{s}^{ij})^2 \rangle - \langle \mathfrak{s}^{ij} \rangle^2}$ , and regard  $\mathfrak{s}_{\max}^{ij}(T, \mu) \equiv \langle \mathfrak{s}^{ij} \rangle + \Sigma^{ij}$  as a measure of the highest energy of the  $i, j$  scattering at temperature  $T$  and baryon chemical potential  $\mu$ .

In Fig. 7, we show the values of  $\mathfrak{s}_{\max}^{NN}$  on the  $T$ - $\mu$  plane. Recall that the fit to experimental data in the  $NN$  scatterings is by construction valid up to  $\mathfrak{s}^{NN} < (2.04)^2 = 4.16 \text{ GeV}^2$ . However, in fact, our parametrization works well up to slightly higher value  $\mathfrak{s}^{NN} \sim (2.3)^2 = 5.29 \text{ GeV}^2$ . Therefore, we define the borderline of the validity region by temperature and chemical potential that satisfy  $\mathfrak{s}_{\max}^{NN}(T, \mu) = 5.29 \text{ GeV}^2$ . The result is shown on the same figure 7 by a thick solid curve. The maximum temperature is about 130 MeV or slightly smaller than that, while the chemical potential is not restricted up to  $\mu = 1 \text{ GeV}$ . If we perform the same analysis for the  $\pi N$  scattering, the borderline defined by  $\mathfrak{s}_{\max}^{\pi N} = 4 \text{ GeV}^2$  locates outside of the region of our interest  $T < 180 \text{ MeV}$ ,

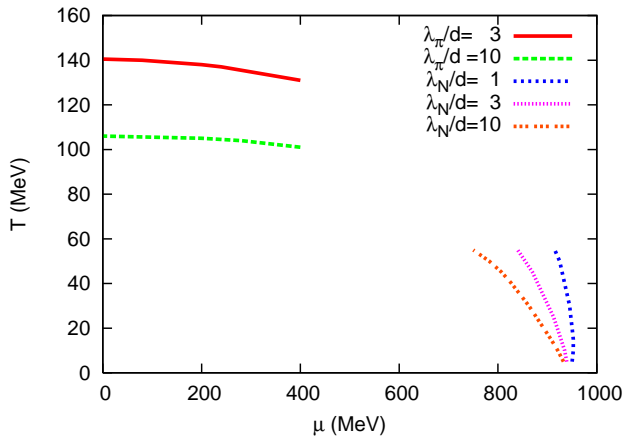


FIG. 8: (Color online) The lines for the ratio  $\lambda_{\pi,N}/d$  in a  $\pi N$  gas. In the region of low density and high temperature, we show only  $\lambda_{\pi}/d$ , while in the region of low temperature and high density,  $\lambda_N/d$ . We may regard the line for  $\lambda/d = 3$  as the border of the validity region of the Boltzmann equations. The line for  $\lambda_{\pi}/d = 1$  is far outside of the  $T$ - $\mu$  region shown here.

$\mu < 1$  GeV. On the other hand, the validity region of the low energy EFT is severely restricted. For example, if we take the maximum value of  $\sqrt{s^{NN}}$  to be 1.88 GeV (beyond which the phenomenological fit starts to deviate from the low energy EFT fit, see Appendix A), then the borderline defined by  $s_{\max}^{NN} = (1.88)^2 = 3.53$  GeV<sup>2</sup> is very close to the horizontal axis (see Fig. 7). Even if we relax the condition to higher value  $s_{\max}^{NN} = (1.90)^2 = 3.61$  GeV<sup>2</sup>, allowed region is still very narrow.

Let us also examine the validity condition for the Boltzmann equations. The criterion is again given by Eq. (28), but now pion's mean-free path should be modified in the presence of nucleons, and we have to separately consider nucleon's mean-free path, too. According to classical transport theories, the mean-free path of  $i$ -th component in a mixed gas is modified as [25]

$$\lambda_i = \frac{\lambda_i^0}{1 + \sum_{j \neq i} \sqrt{\frac{1+m_i/m_j}{2}} \frac{\sigma_{ij} n_j}{\sigma_{ii} n_i}}, \quad (35)$$

where  $\lambda_i^0 = 1/n_i \sigma_i$  is the mean-free path of a pure gas of  $i$ -th component, and  $\sigma_{ij}$  is the cross section between  $i$ -th and  $j$ -th components. Therefore, the mean-free paths of pions and nucleons are respectively given by

$$\lambda_{\pi} = \frac{1}{n_{\pi} \sigma_{\pi\pi} + n_N \sigma_{\pi N} \sqrt{\frac{1+m_{\pi}/m_N}{2}}}, \quad (36)$$

$$\lambda_N = \frac{1}{n_N \sigma_{NN} + n_{\pi} \sigma_{\pi N} \sqrt{\frac{1+m_N/m_{\pi}}{2}}}. \quad (37)$$

Consider the condition for nucleons. If one takes  $\sigma_{NN} \sim 40$  mb as a typical value of the  $NN$  cross section

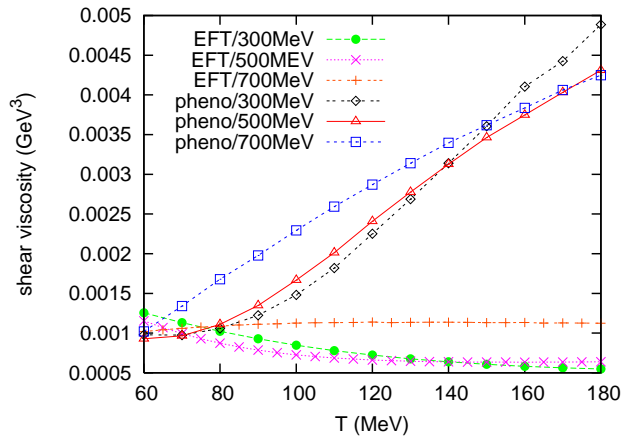


FIG. 9: (Color online) Temperature dependence of the shear viscosity coefficient  $\eta$  of a  $\pi N$  gas at different values of chemical potential  $\mu = 300, 500, 700$  MeV. Comparison is made between the results of the low energy EFT and the phenomenological amplitudes.

(twice of the saturating value at high energy, see Fig. 1) and uses  $d \sim 1/m_{\pi}$  again for the interaction range, then the condition for nucleons  $\lambda_N \gg d$  can be estimated as  $n_N \ll m_{\pi}/\sigma_{NN} \simeq n_N^0$  with  $n_N^0 = 0.157$  fm<sup>-3</sup> being the normal nuclear density. This condition is physically quite reasonable since we do not expect standard Boltzmann description useful at normal nuclear matter density. To obtain more precise restriction depending on  $T$  and  $\mu$ , we need to use Eqs. (36) and (37) and estimate each condition by replacing  $\sigma$  and  $n$  by their thermal averages. In Fig. 8, we show the lines for several values of the ratio  $\lambda/d$  in the  $T$ - $\mu$  plane. For simplicity, we used  $d = 1/m_{\pi}$  for both pions and nucleons. In the region of low baryon density where pions are dominant degrees of freedom for transport phenomena, we show the ratio for pions  $\lambda_{\pi}/d$ . The line for  $\lambda_{\pi}/d = 3$  (solid line) is consistent with the previous result shown in Fig. 3. We may regard this line as the border of the validity of the Boltzmann equations at low densities. On the other hand, at large chemical potential and low temperature, transport phenomena is dominated by nucleons. The lines for the ratio  $\lambda_N/d = 1, 3, 10$  are shown in the figure. We may again regard the line  $\lambda_N/d = 3$  as the borderline, which reaches at  $(T, \mu) = (0, 950\text{MeV})$ . This condition is more restrictive than that of Fig. 7.

Combining these two analyses, we may conclude that our framework is valid in a wide region of the  $T$ - $\mu$  plane, whose boundary is roughly given by (a quarter of) the elliptic curve connecting  $(T, \mu) \sim (130\text{MeV}, 0)$  and  $(0, 950\text{MeV})$ . The first point (130MeV, 0) is specified by the measure of the highest scattering energy squared, and the last point (0, 950MeV) is from the validity limit of the Boltzmann equations.

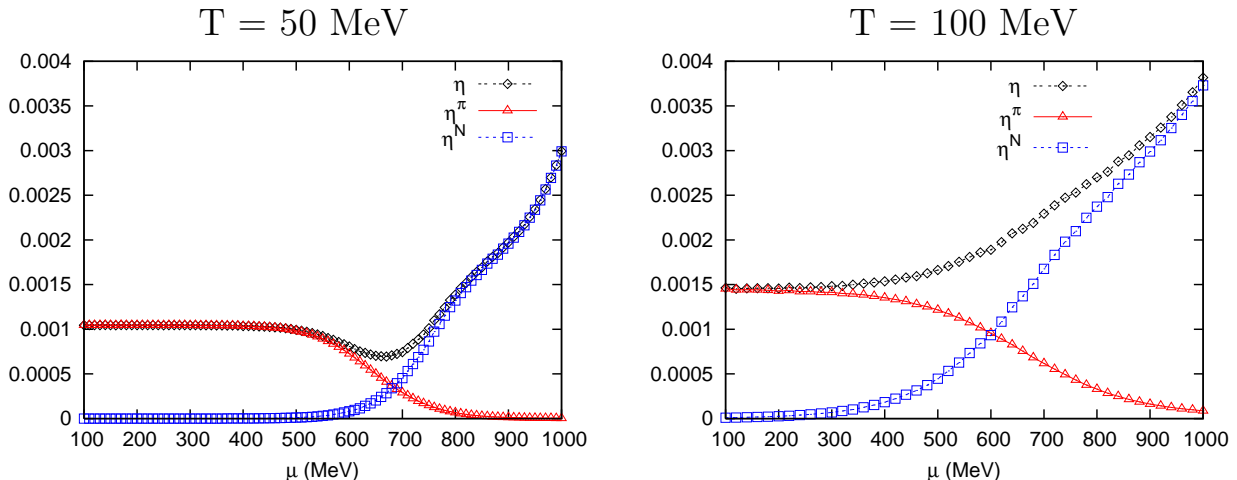


FIG. 10: (Color online)  $\mu$  dependence of  $\eta$  at  $T = 50\text{MeV}$  (left) and  $T = 100\text{MeV}$  (right), and its decomposition  $\eta = \eta^\pi + \eta^N$ .

## 2. Shear viscosity coefficient $\eta$

In Fig. 9, we show temperature dependence of  $\eta$  at different values of chemical potential  $\mu = 300, 500, 700$  MeV. Comparison is made between the results of the low energy EFT and the phenomenological amplitudes. These temperature dependence is qualitatively consistent with the previous results of the pion gas (see Fig. 4). As for the  $\mu$  dependence, however, the shear viscosity coefficient shows nontrivial behavior. In particular, in the window  $80 \text{ MeV} < T < 130 \text{ MeV}$ , it *increases* with increasing  $\mu$ . This is not quite understandable at first because we expect that the cross section of  $\pi\pi$  scattering will effectively enhance in the presence of nucleons while the effects of nucleon viscosity may be ignored at lower density, meaning that the shear viscosity will decrease. To understand what really happens when  $\mu \neq 0$ , let us again consider a rough estimate of the shear viscosity of a mixed gas. Let the shear viscosity coefficient of a pure gas of particle species  $i$  be  $\eta_0^i = n_i \bar{p}_i \lambda_i^0 / 3$  where  $n_i$  is the number density,  $\bar{p}_i$  is the average momentum, and  $\lambda_i^0$  is the mean-free path. Then the shear viscosity coefficient for  $n$  component gas is given by the sum of each viscosity  $\eta_0^i$  with modified mean-free path  $\lambda_i$  given in Eq. (35) [25]:

$$\eta_{\text{mix}} = \sum_i \eta_0^i \frac{\lambda_i}{\lambda_i^0}.$$

Thus for the  $\pi N$  gas mixture, we obtain

$$\begin{aligned} \eta &= \eta^\pi + \eta^N \\ &\simeq \frac{\eta_0^\pi}{1 + \frac{1}{\sqrt{2}} \left( \frac{\sigma_{\pi N}}{\sigma_{\pi\pi}} \right) \left( \frac{n_N}{n_\pi} \right)} + \frac{\eta_0^N}{1 + \sqrt{\frac{m_N}{2m_\pi}} \left( \frac{\sigma_{\pi N}}{\sigma_{NN}} \right) \left( \frac{n_\pi}{n_N} \right)}, \end{aligned} \quad (38)$$

where we have used the approximation  $m_\pi/m_N \ll 1$ . In the two extreme limits  $n_N/n_\pi \rightarrow 0$  and  $\infty$ , the formula (38) reduces to  $\eta_0^\pi$  and  $\eta_0^N$ , respectively. Therefore, this

formula interpolates a pure pion gas at low  $\mu$  and a pure nucleon gas at high  $\mu$ . Notice that the pion contribution  $\eta^\pi$  is always smaller than  $\eta_0^\pi$  due to the presence of  $\pi N$  interaction, as we alluded before in relation to Eq. (21). This is exactly what we expected. On the other hand, it is not straightforward to predict the behavior of the total shear viscosity. If one plots the rough estimate (38) as a function of  $n_N/n_\pi$  assuming that the cross sections are constant and are of the same order, one finds that  $\eta$  decreases at small values of  $n_N/n_\pi$  (small  $\mu$ ), but turns into increase at large  $n_N/n_\pi$  (large  $\mu$ ). If one changes the numerical value of cross sections a little, then the curve turns into monotonic increase. In fact, both can happen in reality depending on temperature. In Fig. 10, we have plotted  $\eta$  at  $T = 50 \text{ MeV}$  and  $100 \text{ MeV}$  as a function of  $\mu$ . While the total viscosity behaves differently in these two panels, one can see monotonic decrease (increase) of  $\eta^\pi$  ( $\eta^N$ ), namely, the interplay between  $\eta^\pi$  and  $\eta^N$  at both temperatures. Therefore, the increase of  $\eta$  with increasing  $\mu$  observed in Fig. 9 can be understood as a result of enhancement of  $\eta^N$ .

## 3. The ratio $\eta/s$

Figure 11 shows temperature dependence of the ratio  $\eta/s$  of the  $\pi N$  gas at different values of baryon chemical potential  $\mu = 300, 500, 700$  MeV. The left-hand side is the results of the low energy EFT, while the right-hand side, the phenomenological amplitudes. The ratio  $\eta/s$  shows qualitatively the same behavior as in the pion gas system (Fig. 5): (i) Both the results (EFT and phenomenological amplitudes) are monotonically decreasing functions of  $T$ , (ii)  $(\eta/s)_{\text{EFT}} > (\eta/s)_{\text{pheno}}$  at lower  $T$  while opposite at higher  $T$ , and (iii) the ratio of the EFT violates the KSS bound at around  $T \sim T_c$  while that of the phenomenological amplitudes does not. Notice that the inclusion of chemical potential works to re-

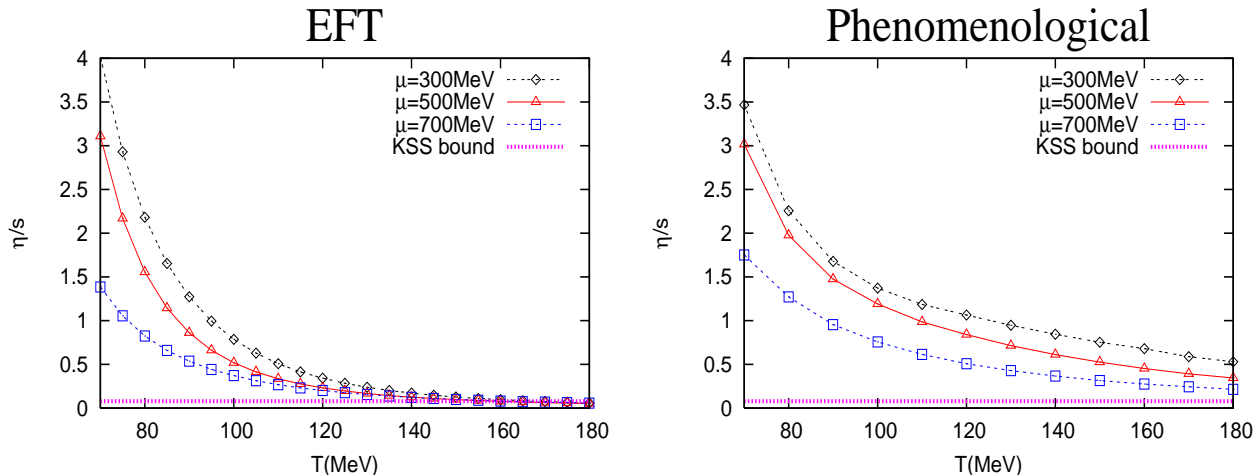


FIG. 11: (Color online) The ratio  $\eta/s$  of a  $\pi N$  system plotted as a function of temperature  $T$  at different values of baryon chemical potential  $\mu = 300, 500, 700$  MeV. (Left) results of low energy EFT, (Right) results of phenomenological amplitudes.

duce the value of  $\eta/s$ . As a result, for the ratio of the EFT, the temperature at which the curve cuts the KSS bound becomes smaller. On the other hand, for the result of the phenomenological amplitudes, the flattening of the curves seems to occur at lower temperature with increasing  $\mu$ . If this is indeed the symptom of crossover transition as we discussed before, one can say that the (pseudo) critical temperature  $T_c$  will decrease with increasing  $\mu$ , which is consistent with what we know from lattice simulations or effective models. [33]

Our result  $(\eta/s)_{\text{pheno}} \sim 0.5 - 0.4$  at  $\mu = 700$  MeV and  $T \sim 100 - 140$  MeV is consistent with that of “URASiMA” (Ultra-Relativistic AA collision Simulator based on Multiple scattering Algorithm)[18] which is a Monte-Carlo event generator of hadronic collisions. It includes both elastic and inelastic scatterings whose cross sections are given by experimental data. The numerical coincidence of the ratio from different frameworks is very interesting. In fact, the essential difference of URASiMA from our framework is the presence of inelastic collisions. But as far as we consider small deviation from thermal equilibrium, inelastic collisions which will change particle numbers (such as  $\pi\pi \rightarrow \pi\pi\pi$  or  $\pi N \rightarrow \pi\pi N$ ) would not be so important, and it seems reasonable to obtain the same result from two different frameworks.

As we already saw in Fig. 9, the shear viscosity coefficient *increases* in the window  $80 \text{ MeV} < T < 130 \text{ MeV}$  with increasing  $\mu$ . However, in the same window, the ratio *does* decrease. This clearly implies that the reduction of  $\eta/s$  at  $T \sim 80 - 130$  MeV is due to the increase of entropy.

In Fig. 12, we show the  $\mu$  dependence of the ratio  $\eta/s$  at temperature  $T = 50, 100$  MeV (left) and at low temperature  $T = 10$  MeV (right). Recall that the ratio decreases with increasing  $\mu$  in Fig. 11 where  $T \geq 70$  MeV was shown. This is consistent with the left figure, and in agreement with our original expectation as we mentioned in Introduction. On the other hand, the right

figure shows a new structure: There is a valley at large  $\mu \sim 950$  MeV. We will discuss later the physical implication of this structure.

Let us comment again the point made in the last paragraph of the previous subsection. The ratio  $\eta/s$  becomes less than 0.3 at  $T \gtrsim 140$  MeV and  $\mu = 700$  MeV. This is small enough and is close to the KSS bound  $\eta/s \sim 0.1$  compared to other systems such as water. However, as shown in Figs. 9 and 10, the shear viscosity itself grows as the system approaches phase boundary ( $T \rightarrow T_c, \mu \rightarrow \mu_c$ ). Therefore, even if the ratio is small enough, the  $\pi N$  system cannot be treated, strictly speaking, as a perfect fluid with  $\eta = 0$ . Sometimes ideal hydrodynamics is used to describe the matter after hadronization in heavy-ion collisions, but one will have to take into account the effects of viscosity for a realistic simulation.

#### 4. Valley structure at large $\mu$ and low $T$

In the right panel of Fig. 12 (low temperature  $T = 10$  MeV), we pointed out a valley structure at high baryon chemical potential, which was not seen in higher temperature (left panel). Let us look at this new structure in more detail and examine its possible interpretation. We recall again Ref. [6], where it was suggested that the ratio  $\eta/s$  would give a minimum at the phase transition temperature. If this is true for other control parameters, in particular, chemical potential, and if there is phase transition under the change of chemical potential, it is natural to expect that the ratio would exhibit a valley structure with its minimum at the critical chemical potential  $\mu_c$ . In other words, if one finds a valley structure in the  $\mu$  direction, one can expect some kind of phase transition around the minimum. This is what we observed in Fig. 12. Then, what kind of phase transition could be related to this valley structure? The valley locates at



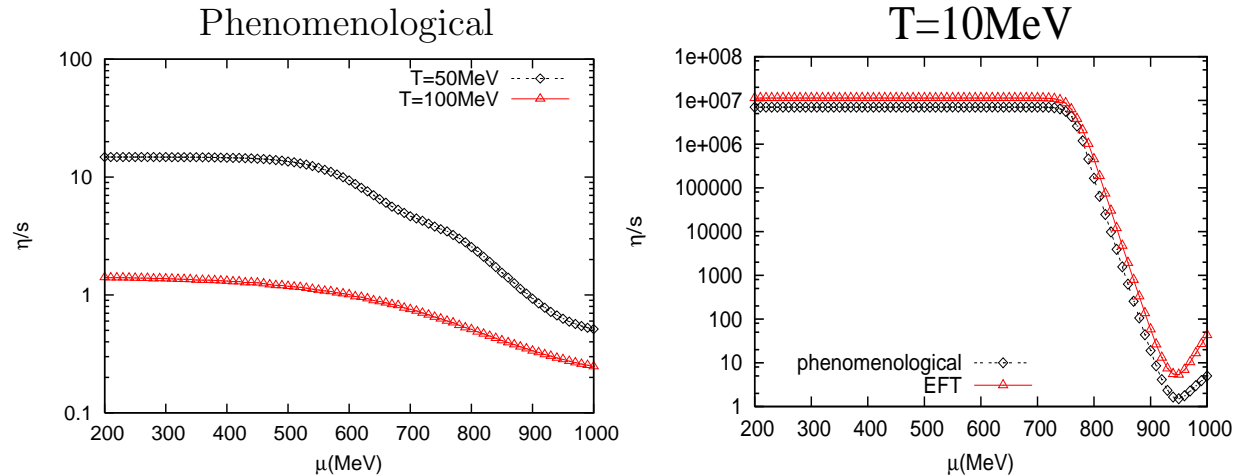


FIG. 12: (Color online)  $\mu$  dependence of  $\eta/s$ : (left): the results of the phenomenological amplitudes at higher temperature  $T = 50, 100$  MeV, (right): the results at lower temperature  $T = 10$  MeV.

low temperature  $T < 20$  MeV and at high chemical potential  $\mu \sim 950$  MeV (which is however not enough for the quark-hadron phase transition). This is the region where we can see the *liquid-gas phase transition*. [34] At low  $T < 20$  MeV and around normal nuclear density, there is a critical line (possibly first order) separating a nucleon gas phase and a nuclear matter (liquid). This line terminates at around  $T \sim 15$  MeV [27], and above that temperature, there is no distinction between a gas and a liquid. Therefore, if the valley indeed corresponds to the liquid-gas phase transition, it should disappear when the temperature go far beyond  $T \sim 15$  MeV. In Fig. 13, we show the transition of the valley structure from  $T = 5$  MeV up to  $T = 20$  MeV. The right panel is the results of the phenomenological amplitudes. Clearly, with increasing temperature, the valley becomes shallow, which supports the interpretation that the valley structure indeed corresponds to the liquid-gas phase transition. There are several comments about this.

- Although the liquid-gas phase transition is a phenomenon in the hadronic phase, it is not obvious whether the Boltzmann equations (valid for a dilute gas) correctly describe the transition to liquid phase. Notice that the region where liquid-gas phase transition takes place is close to the border of the validity region of the Boltzmann equations, and thus it is not surprising that there might exist another phase (i.e., liquid phase) outside the region of validity. Still, it would be safe to reserve that reliable information from our analysis should be only the tendency towards phase transition. We do not expect we can describe precise structure of phase transition such as the order of transition and the temperature dependence of the critical chemical potential  $\mu_c(T)$  (Our result is that the minimum of the valley moves to the right with increasing  $T$ , as opposed to common expectation). In order to describe the

transition correctly, we will have to include the effects of higher-order correlations to the Boltzmann equations, or start from different models (such as the  $\sigma$ - $\omega$  model) which are more appropriate for nuclear matter, both of which, however, are beyond the scope of the present paper.

- As mentioned in Introduction, a similar valley structure was already reported in the calculation with the low energy EFT [16] and the authors of Ref. [16] claim that it is related to the liquid-gas phase transition. We have done the same calculation with our own parametrizations of low energy EFT, and obtained consistent results with Ref. [16] as shown in the left panel of Fig. 13. Unlike the results of the phenomenological amplitudes (the right panel), the valley persists even at higher temperature. As we repeated several times, since the range of validity of the low energy EFT is severely restricted (see the discussion about Fig. 7), it is quite dangerous to draw any conclusions about the physics outside of the validity region. However, a similar valley structure is observed even in our calculation with the phenomenological amplitudes, and thus our calculation partially supports the results of low energy EFT.

- Since the entropy in our calculation is evaluated by using free particle distributions  $f_0^{\pi,N}(p)$ , there is no information about phase transition in the denominator of  $\eta/s$ . However, if there is a real phase transition, entropy will of course show nontrivial change around  $T_c$  or  $\mu_c$ . For example, in the liquid-gas transition of water, both the shear viscosity and the entropy have nontrivial structure around  $T_c$ , and contribute to give a convex shape of the ratio  $\eta/s$ . We emphasize that, in our calculation, the valley structure of  $\eta/s$  is not the result of entropy. If we treated actual entropy, the structure would emerge in more pronounced way.

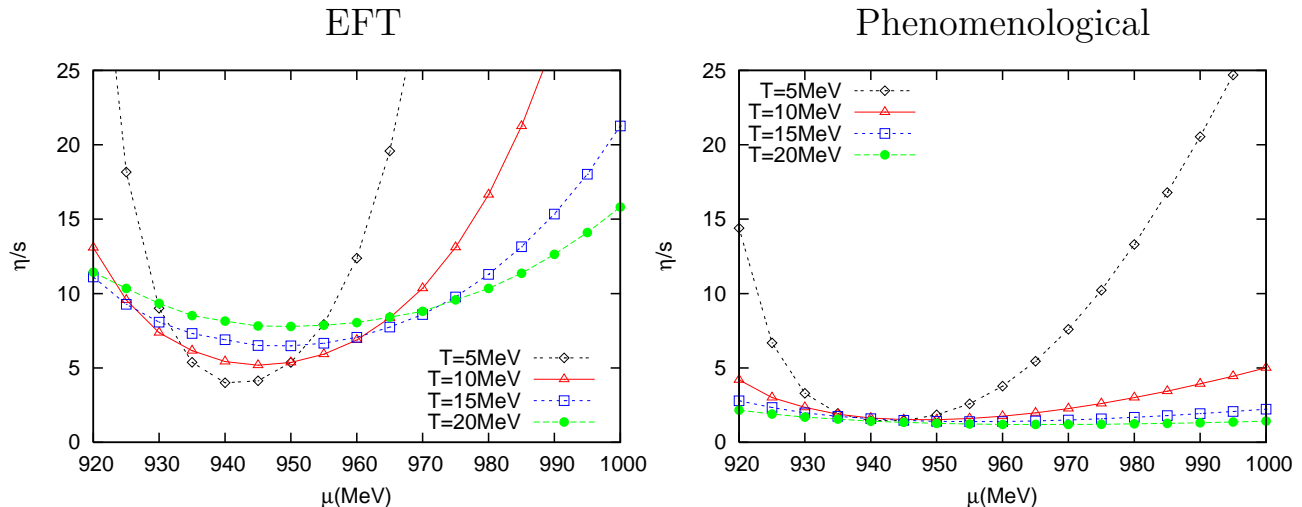


FIG. 13: (Color online) Temperature dependence of the valley structure of  $\eta/s$  at relatively high chemical potential. Only the results at low temperature  $T = 5, 10, 15, 20$  MeV are shown. (Left): Low energy EFT, (Right): Phenomenological amplitudes.

#### IV. SUMMARY

We have performed a detailed calculation of the shear viscosity coefficient  $\eta$  and the viscosity to entropy ratio  $\eta/s$  in a wide region of the hadronic  $T$ - $\mu$  plane. Our formalism is based on the relativistic quantum Boltzmann equations, and we found that it is very important to use phenomenological amplitudes for the scattering amplitudes in the collision terms in order to obtain reliable results. On the other hand, the validity region of the low energy effective field theories is severely restricted, and reliable results based on them are also limited to a small region of  $T$ - $\mu$  plane. We found that the ratio  $\eta/s$  decreases (for  $T \gtrsim 20$  MeV) under the inclusion of nucleon degrees of freedom, but still keeps above the conjectured KSS bound  $\eta/s = 1/4\pi$  in the region we investigated ( $T < 180$  MeV,  $\mu < 1000$  MeV). Since the shear viscosity coefficient itself increases with increasing temperature, the behavior of the ratio is largely due to the entropy. At low temperature  $T \lesssim 15$  MeV and high baryon chemical potential  $\mu \sim 950$  MeV, we found a valley structure in the ratio. There is some argument about the relationship between such structure and phase transition, and we expect that the valley structure found in our calculation would correspond to the liquid-gas phase transition.

#### Acknowledgments

The authors are grateful to E. Nakano for discussion and to H. Hayakawa for explaining them the essence of

the Chapman-Enskog method. Two of the authors (KI and HO) are thankful to S. Muroya for his encouragements and constructive comments. Lastly, one of the authors (HO) thanks A. Dote for useful advises on the fitting method of experimental data.

#### APPENDIX A: PHENOMENOLOGICAL AMPLITUDES

In this Appendix, we explain the phenomenological amplitudes we used in the kinetic equations. Since the scattering amplitude (squared) is related to the differential cross section in the CM frame as

$$\left(\frac{d\sigma}{d\Omega}\right) = \frac{1}{64\pi^2 s} |M|^2, \quad (\text{A1})$$

with  $s$  being the Mandelstam variable (scattering energy squared), we discuss only the differential cross sections.

##### 1. $\pi\pi$ scattering

Consider the partial-wave expansion of the isospin averaged  $\pi\pi$  elastic differential cross section. Taking up to  $p$ -wave scattering ( $\ell = 1$ ) yields a very nice description of the experimental data:



$$\begin{aligned}
\left(\frac{d\sigma}{d\Omega}\right)^{\pi\pi} &= \frac{1}{\sum_{I'}(2I'+1)} \sum_{I=0}^2 (2I+1) \frac{4}{q_{\text{cm}}^2} \sum_{\ell=0,1} \left| (2\ell+1) e^{i\delta_\ell^I} \sin \delta_\ell^I P_\ell(\cos \theta_{\text{cm}}) \right|^2 \\
&= \frac{4}{q_{\text{cm}}^2} \left( \frac{1}{9} \sin^2 \delta_0^0 + \frac{5}{9} \sin^2 \delta_0^2 + \frac{3}{9} \cdot 9 \sin^2 \delta_1^1 \cos^2 \theta_{\text{cm}} \right), \tag{A2}
\end{aligned}$$

where 4 in the overall factor comes from the identical factor,  $\theta_{\text{cm}}$  and  $q_{\text{cm}}$  are the scattering angle and the magnitude of momentum in the CM frame, and  $P_\ell$  is the  $\ell$ -th order Legendre polynomial ( $P_0(x) = 1$ ,  $P_1(x) = x$ ). The numerical factors in the last line are from isospin  $I$  and orbital angular momentum  $\ell$ . For example, the last term corresponds to  $I = \ell = 1$  scattering and thus  $(3/9) \cdot 9$  is from the isospin weight  $(2I+1)/\sum_{I'}(2I'+1) = 3/9$  for  $I = 1$  and  $(2\ell+1)^2 = 9$  for  $\ell = 1$ . The phase shift  $\delta_\ell^I$  depends on  $\ell$  and  $I$ . Since the total wavefunction of a  $\pi\pi$  system must be symmetric under the exchange, only three phase shifts  $(I, \ell) = (0, 0), (1, 1), (2, 0)$  are possible. It is known that the energy dependence of the phase shifts are well parametrized by the following function [28]:

$$\begin{aligned}
\tan \delta_\ell^I &= \sqrt{1 - \frac{4m_\pi^2}{s}} q_{\text{cm}}^{2\ell} \left( A_\ell^I + B_\ell^I q_{\text{cm}}^2 + C_\ell^I q_{\text{cm}}^4 + D_\ell^I q_{\text{cm}}^6 \right) \\
&\quad \times \left( \frac{4m_\pi^2 - s_\ell^I}{s - s_\ell^I} \right), \tag{A3}
\end{aligned}$$

where the parameters are determined to fit the data up to  $\sqrt{s} = 1.15$  GeV ( $q_{\text{cm}} \sim 550$  MeV) and are shown in table II:

TABLE II:

	$(I, \ell) = (0, 0)$		$(I, \ell) = (1, 1)$		$(I, \ell) = (2, 0)$
$A_0^0$	$2.25 \times 10^{-1}$	$A_1^1$	$3.63 \times 10^{-2}$	$A_0^2$	$-3.71 \times 10^{-2}$
$B_0^0$	$2.46 \times 10^{-1}$	$B_1^1$	$1.34 \times 10^{-4}$	$B_0^2$	$-8.55 \times 10^{-2}$
$C_0^0$	$-1.67 \times 10^{-2}$	$C_1^1$	$-6.98 \times 10^{-5}$	$C_0^2$	$-7.54 \times 10^{-3}$
$D_0^0$	$-6.40 \times 10^{-4}$	$D_1^1$	$1.41 \times 10^{-6}$	$D_0^2$	$-1.99 \times 10^{-4}$
$s_0^0$	36.7	$s_1^1$	30.7	$s_0^2$	-11.9

In this table, dimensionful parameters are redefined so that the mass dimension is provided by  $m_\pi$ . For example, since  $B_0^0$  has mass dimension  $-2$ , we define  $B_0^0 \equiv b_0^0/m_\pi^2$  and  $b_0^0 = 2.46 \times 10^{-1}$ . This phenomenological parametrization describes the experimental data very well. We use this for the  $\pi\pi$  scattering amplitude.

## 2. $\pi N$ scattering

Let us now turn to the  $\pi N$  scattering. Consider the partial-wave expansion of the isospin averaged  $\pi N$  differ-

ential cross section:

$$\begin{aligned}
\left(\frac{d\sigma}{d\Omega}\right)^{\pi N} &= \frac{1}{q_{\text{cm}}^2} \sum_{\ell=0}^{2\ell_{\text{max}}} \left( \frac{2}{6} Q_\ell^{I=1/2}(q_{\text{cm}}) + \frac{4}{6} Q_\ell^{I=3/2}(q_{\text{cm}}) \right) \\
&\quad \times P_\ell(\cos \theta). \tag{A4}
\end{aligned}$$

The coefficients

$$C_\ell(q_{\text{cm}}) \equiv \frac{2}{6} Q_\ell^{1/2}(q_{\text{cm}}) + \frac{4}{6} Q_\ell^{3/2}(q_{\text{cm}})$$

are functions of  $q_{\text{cm}}$  and are determined from the experimental data. More precisely, each function  $C_\ell$  is expressed by a superposition of 30 Gaussians: For example, for  $\ell = 0$ , we use

$$\begin{aligned}
C_{\ell=0}(q_{\text{cm}}) &= \sum_{n=1}^{15} A_n \exp \left\{ - \left( \frac{q_{\text{cm}} - 100 \text{MeV}}{60^n \text{MeV}} \right)^2 \right\} \\
&\quad + \sum_{n=16}^{30} A_n \exp \left\{ - \left( \frac{q_{\text{cm}} - 800 \text{MeV}}{60^n \text{MeV}} \right)^2 \right\},
\end{aligned}$$

where positions and widths of Gaussians are found by trial and error. We use different values of positions and widths for different  $\ell$ . This kind of technique is sometimes used in describing nuclear many body wavefunctions. By using these functions and taking the maximum angular momentum  $2\ell_{\text{max}} = 8$ , we can fit the experimental data [29] up to  $\sqrt{s} = 2$  GeV ( $q_{\text{cm}} \sim 770$  MeV). Notice that this parametrization works very well at relatively high scattering energies, but in fact its quality becomes worse at small scattering energies. This is due to the factor  $1/q_{\text{cm}}^2$  in Eq. (A4). If one absorbed this factor into the coefficients and performed the same Gaussian fitting, quality of the fit would be better even at low scattering energies. However, we decided to start from the conventional expression shown in Eq. (A4), and to find another parametrization for the low energy data. We have interpolated the parametrization proposed in Ref. [30] which is compactly represented for the scattering amplitude:

$$\begin{aligned}
M_{\pi N} &= b_0 + b_1(\vec{t} \cdot \vec{\tau}) + (c_0 + c_1(\vec{t} \cdot \vec{\tau}))(\vec{q} \cdot \vec{q}') \\
&\quad + i(d_0 + d_1(\vec{t} \cdot \vec{\tau}))\vec{\sigma} \cdot (\vec{q} \times \vec{q}'),
\end{aligned}$$

where  $\vec{t}$  and  $\vec{\tau}/2$  are the isospin vectors of a pion and a nucleon respectively,  $\vec{q}$  and  $\vec{q}'$  are the momenta of incoming particles in the CM frame, and lastly  $\vec{\sigma}$  is the Pauli

TABLE III:

$b_0$	-0.010	$b_1$	-0.091
$c_0$	0.208	$c_1$	0.175
$d_0$	-0.190	$d_1$	-0.069

matrix. The parameters are determined as shown in table III (dimensionful parameters are again redefined by using  $m_\pi$  so that they become dimensionless).

These two different parametrizations are smoothly matched at  $\sqrt{s} = 1101$  MeV ( $q_{\text{cm}} = 79$  MeV), giving a very nice parametrization of the experimental data for a wide region of scattering energies.

### 3. $NN$ scattering

Let us finally discuss the  $NN$  scattering. In the text we discussed only the  $s$ -wave scattering, but here we treat arbitrary orbital angular momentum. We define the spin-isospin averaged  $NN$  differential cross section

$$\left(\frac{d\sigma}{d\Omega}\right)_{\text{averaged}}^{NN} \equiv \frac{1}{16} \left\{ \left(\frac{d\sigma}{d\Omega}\right)^{0,0} + 3 \left(\frac{d\sigma}{d\Omega}\right)^{1,0} + 3 \left(\frac{d\sigma}{d\Omega}\right)^{0,1} + 9 \left(\frac{d\sigma}{d\Omega}\right)^{1,1} \right\}, \quad (\text{A5})$$

$$\left(\frac{d\sigma}{d\Omega}\right)_{\text{averaged}}^{NN} = \frac{1}{q_{\text{cm}}^2} \left[ \sum_{\ell=\text{even}} \left\{ \frac{3}{16} E_\ell^{1,0} + \frac{3}{16} E_\ell^{0,1} \right\} P_\ell(\cos\theta) + \sum_{\ell=\text{odd}} \left\{ \frac{1}{16} O_\ell^{0,0} + \frac{9}{16} O_\ell^{1,1} \right\} P_\ell(\cos\theta) \right]. \quad (\text{A10})$$

When  $\ell = 0$ , this gives the spin-isospin averaged scattering amplitude used in the parametrization of low energy effective theory.

Restriction to the  $s$ -wave alone may be a good approximation at low scattering energy, but to obtain a parametrization which describes the data in much wider range of energies, we have to include larger  $\ell$ . To do this, we again perform the partial-wave expansion of the spin-isospin averaged differential cross section (A5) and fit the energy-dependent coefficients by using the Gaussian superposition. We define the coefficients  $D_\ell(q_{\text{cm}})$  similarly to Eq. (A4):

$$\left(\frac{d\sigma}{d\Omega}\right)_{\text{averaged}}^{NN} = \frac{1}{q_{\text{cm}}^2} \sum_{\ell} D_\ell(q_{\text{cm}}) P_\ell(\cos\theta). \quad (\text{A11})$$

Since the low energy data are already described well by the parametrization (24) and the parameters given in table I, we adopt them as the low energy part of the global parametrization. We use them up to  $q_{\text{cm}} = 6.76$  MeV ( $\sqrt{s} = 1.88$  GeV), and beyond that, we switch to the

where  $16 = \sum_{I=0,1} (2I+1) \sum_{S=0,1} (2S+1)$  and  $(d\sigma/d\Omega)^{I,S}$  in the right-hand side are the differential cross sections with isospin  $I$  and spin  $S$  specified. One can further decompose each contribution depending on the value of orbital angular momentum  $\ell$ . (Notice that the total  $NN$  system must be antisymmetric under the exchange of two particles:  $(-1)^{\ell+S+I} = -1$ .)

$$\left(\frac{d\sigma}{d\Omega}\right)^{0,0} = \frac{1}{q_{\text{cm}}^2} \sum_{\ell=\text{odd}} O_\ell^{0,0}(q_{\text{cm}}) P_\ell(\cos\theta), \quad (\text{A6})$$

$$\left(\frac{d\sigma}{d\Omega}\right)^{1,0} = \frac{1}{q_{\text{cm}}^2} \sum_{\ell=\text{even}} E_\ell^{1,0}(q_{\text{cm}}) P_\ell(\cos\theta), \quad (\text{A7})$$

$$\left(\frac{d\sigma}{d\Omega}\right)^{0,1} = \frac{1}{q_{\text{cm}}^2} \sum_{\ell=\text{even}} E_\ell^{0,1}(q_{\text{cm}}) P_\ell(\cos\theta), \quad (\text{A8})$$

$$\left(\frac{d\sigma}{d\Omega}\right)^{1,1} = \frac{1}{q_{\text{cm}}^2} \sum_{\ell=\text{odd}} O_\ell^{1,1}(q_{\text{cm}}) P_\ell(\cos\theta). \quad (\text{A9})$$

Inserting these into Eq. (A5), we obtain the spin-isospin averaged differential cross section separately for even and odd  $\ell$ :

partial-wave expansion (A11). For actual fitting of the experimental data [31], we divide the rest of the region into two:

- (i)  $6.762 \text{ MeV} < q_{\text{cm}} < 48.76 \text{ MeV}$   
( $1876 \text{ MeV} < \sqrt{s} < 1879 \text{ MeV}$ )
- (ii)  $48.76 \text{ MeV} < q_{\text{cm}} < 405 \text{ MeV}$   
( $1879 \text{ MeV} < \sqrt{s} < 2043 \text{ MeV}$ )

In each region, we determine the coefficient  $D_\ell(q_{\text{cm}})$  similarly as in the case for  $\pi N$  scattering, so that the curve is smoothly connected at the matching points  $q_{\text{cm}} = 6.762$  MeV and  $q_{\text{cm}} = 48.76$  MeV. In region (i), the highest value of the angular momentum is taken to be 6, while in region (ii), much higher value 16. We performed the fit up to  $q_{\text{cm}} = 405$  MeV ( $\sqrt{s} = 2043$  MeV).

## APPENDIX B: SOLVING THE LINEARIZED BOLTZMANN EQUATIONS

In this Appendix, we discuss how to solve the Boltzmann equations (1) and (2). First of all, recall that the lo-

cal equilibrium state is defined by the distributions  $f_0^{\pi,N}$  which make the collision terms (the right hand side of the Boltzmann equations) vanishing [see Eqs. (6), (7)]. However it should be noticed that the local equilibrium is *not* the solution to the Boltzmann equations: Indeed, the parameters  $T$ ,  $\mu$  and  $V^\mu$  characterizing  $f_0^{\pi,N}$  are dependent on the coordinates, which implies that the left

hand side of the Boltzmann equations (which have coordinate derivative  $\partial_\mu$ ) do not vanish. With this in mind, the Boltzmann equations linearized with respect to the deviations  $\delta f^{\pi,N}$  from the local equilibrium  $f_0^{\pi,N}(x,p)$  can read as follows (leading order of the left hand side does not contain  $\delta f^{\pi,N}$ ):

$$\frac{p^\mu}{E_p^\pi} \partial_\mu f_0^\pi = \mathcal{C}^{\pi\pi}[\delta f^\pi, f_0^\pi] + \mathcal{C}^{\pi\pi}[f_0^\pi, \delta f^\pi] + \mathcal{C}^{\pi N}[\delta f^\pi, f_0^N] + \mathcal{C}^{\pi N}[f_0^\pi, \delta f^N], \quad (\text{B1})$$

$$\frac{p^\mu}{E_p^N} \partial_\mu f_0^N = \mathcal{C}^{NN}[\delta f^N, f_0^N] + \mathcal{C}^{NN}[f_0^N, \delta f^N] + \mathcal{C}^{N\pi}[\delta f^N, f_0^\pi] + \mathcal{C}^{N\pi}[f_0^N, \delta f^\pi], \quad (\text{B2})$$

where the notation for the collision term is for example (see Eq. (3))

$$\begin{aligned} \mathcal{C}^{\pi\pi}[\delta f^\pi, f_0^\pi] &\equiv \mathcal{C}^{\pi\pi}[f_0^\pi + \delta f^\pi, f_0^\pi] - \mathcal{C}^{\pi\pi}[f_0^\pi, f_0^\pi] \\ &= \frac{g_\pi}{2} \int d\Gamma^{\pi\pi} \left\{ \delta f_1^\pi f_{02}^\pi (1 + f_{03}^\pi) (1 + f_{0p}^\pi) + f_{01}^\pi f_{02}^\pi \delta f_3^\pi (1 + f_{0p}^\pi) \right. \\ &\quad \left. - \delta f_1^\pi (1 + f_{02}^\pi) f_{03}^\pi f_{0p}^\pi - (1 + f_{01}^\pi) (1 + f_{02}^\pi) \delta f_3^\pi f_{0p}^\pi \right\}. \end{aligned} \quad (\text{B3})$$

This corresponds to the lowest order Chapman-Enskog method. So far, the deviations  $\delta f^{\pi,N}$  are in principle arbitrary, but for the purpose of computing the shear viscosity coefficient  $\eta$ , we can restrict only to the deviations that are directly from the shear  $\partial_i V_j \neq 0$  ( $i \neq j$ ). Thus we ignore any other effects except the shear.

By using the particle number conservation  $\partial_t n = -n \nabla_i V^i$  and the energy-momentum conservation  $\partial_\nu T^{\mu\nu} = 0$ , the left hand sides of Eqs. (B1) and (B2) can be rewritten as

$$\frac{p^\mu}{E_p^\pi} \partial_\mu f_0^\pi(x) = \beta \frac{f_0^\pi(1 + f_0^\pi)}{E_p^\pi} \left( p_i p_j - \frac{\delta_{ij}}{3} p^2 \right) (\nabla^i V^j)_{\text{trl}}, \quad (\text{B4})$$

$$\frac{p^\mu}{E_p^N} \partial_\mu f_0^N(x) = \beta \frac{f_0^N(1 - f_0^N)}{E_p^N} \left( p_i p_j - \frac{\delta_{ij}}{3} p^2 \right) (\nabla^i V^j)_{\text{trl}}, \quad (\text{B5})$$

where  $(\nabla^i V^j)_{\text{trl}}$  is defined in Eq. (11). Notice that this functional form was the motivation for defining new quantities  $B^{\pi,N}(p)$  in Eqs. (13), (14). Indeed, with respect to  $B^{\pi,N}(p)$ , the right hand sides of Eqs. (B1) and (B2) can be expressed rather compactly. Introducing further the following notation,

$$B_{ij}^{\pi,N}(p) \equiv \left( \hat{p}_i \hat{p}_j - \frac{\delta_{ij}}{3} \right) B^{\pi,N}(p), \quad (\text{B6})$$

the linearized Boltzmann equations (B1) and (B2) can be expressed as ( $f_{01}^\pi \equiv f_0^\pi(k_1)$ ,  $f_{0p}^\pi \equiv f_0^\pi(p)$ , etc.)

$$\begin{aligned} \frac{f_{0p}^\pi(1 + f_{0p}^\pi)}{E_p^\pi} \left( p_i p_j - \frac{\delta_{ij}}{3} p^2 \right) &= \frac{g_\pi}{2} \int d\Gamma^{\pi\pi} (1 + f_{01}^\pi) (1 + f_{02}^\pi) f_{03}^\pi f_{0p}^\pi \left( B_{ij}^\pi(p) + B_{ij}^\pi(k_3) - B_{ij}^\pi(k_2) - B_{ij}^\pi(k_1) \right) \\ &+ g_N \int d\Gamma^{\pi N} (1 - f_{01}^N) (1 + f_{02}^\pi) f_{03}^N f_{0p}^\pi \left( B_{ij}^\pi(p) + B_{ij}^N(k_3) - B_{ij}^\pi(k_2) - B_{ij}^N(k_1) \right), \end{aligned} \quad (\text{B7})$$

$$\begin{aligned} \frac{f_{0p}^N(1 - f_{0p}^N)}{E_p^N} \left( p_i p_j - \frac{\delta_{ij}}{3} p^2 \right) &= g_\pi \int d\Gamma^{N\pi} (1 + f_{01}^\pi) (1 - f_{02}^N) f_{03}^\pi f_{0p}^N \left( B_{ij}^N(p) + B_{ij}^\pi(k_3) - B_{ij}^N(k_2) - B_{ij}^\pi(k_1) \right) \\ &+ \frac{g_N}{2} \int d\Gamma^{NN} (1 - f_{01}^N) (1 - f_{02}^N) f_{03}^N f_{0p}^N \left( B_{ij}^N(p) + B_{ij}^N(k_3) - B_{ij}^N(k_2) - B_{ij}^N(k_1) \right). \end{aligned} \quad (\text{B8})$$

These are the equations for  $B^{\pi,N}(p)$ . As explained in the text, we solve these equations by restricting  $B^{\pi,N}(p)$

to a finite dimensional functional space. More precisely,

we expand  $B^{\pi,N}(p)$  in terms of orthogonal polynomial functions  $W_{(n)}^{\pi,N}(p)$  [see Eq. (16)] and approximate the series by the first three terms [see Eqs. (19) and (20)]. The expansion coefficients ( $b_{(n)}^{\pi,N}$ ,  $n = 0, 1, 2$ ) in Eqs. (19) and (20) are determined as follows: we multiply Eq. (B7) by  $\frac{1}{(2\pi)^3}(\hat{p}_i\hat{p}_j - \frac{\delta_{ij}}{3})W_{(m)}^{\pi}(p)$  ( $m = 0, 1, 2$ ), Eq. (B8) by

$\frac{1}{(2\pi)^3}(\hat{p}_i\hat{p}_j - \frac{\delta_{ij}}{3})W_{(m)}^N(p)$  ( $m = 0, 1, 2$ ), and integrate them over  $p$ . Then, by using the orthogonal conditions (17), (18), we will obtain six independent equations for the coefficients  $b_{(n)}^{\pi,N}$  ( $n = 0, 1, 2$ ). The resulting equations are still complicated but can be solved in a numerical way.

- 
- [1] For an overview of the RHIC results, see the special volume "First three years of operation of RHIC", Nucl. Phys. A757, issues 1-2 (2005).
- [2] P. Kovtun, D. T. Son and A. O. Starinets, Phys. Rev. Lett. **94**, 111601 (2005) [arXiv:hep-th/0405231].
- [3] S. Gavin and M. Abdel-Aziz, Phys. Rev. Lett. **97**, 162302 (2006) [arXiv:nucl-th/0606061].
- [4] A. Nakamura and S. Sakai, Phys. Rev. Lett. **94**, 072305 (2005) [arXiv:hep-lat/0406009]; Nucl. Phys. A **774**, 775 (2006) [arXiv:hep-lat/0510039]; PoS **LAT2005**, 186 (2006) [arXiv:hep-lat/0510100].
- [5] H. B. Meyer, arXiv:0704.1801 [hep-lat].
- [6] L. P. Csernai, J. I. Kapusta and L. D. McLerran, Phys. Rev. Lett. **97**, 152303 (2006) [arXiv:nucl-th/0604032].
- [7] T. Hirano and M. Gyulassy, Nucl. Phys. A **769**, 71 (2006) [arXiv:nucl-th/0506049].
- [8] S. R. De Groot, W. A. Van Leeuwen and C. G. Van Weert, "Relativistic Kinetic Theory. Principles and Applications," (Amsterdam, Netherlands: North-holland, 1980, 417p)
- [9] S. Gavin, Nucl. Phys. A **435**, 826 (1985).
- [10] M. Prakash, M. Prakash, R. Venugopalan and G. Welke, Phys. Rept. **227**, 321 (1993).
- [11] D. Davesne, Phys. Rev. C **53**, 3069 (1996).
- [12] A. Dobado and S. N. Santalla, Phys. Rev. D **65**, 096011 (2002) [arXiv:hep-ph/0112299].
- [13] A. Dobado and F. J. Llanes-Estrada, Phys. Rev. D **69**, 116004 (2004) [arXiv:hep-ph/0309324].
- [14] J. W. Chen and E. Nakano, Phys. Lett. B **647**, 371 (2007) [arXiv:hep-ph/0604138].
- [15] A. Dobado and F. J. Llanes-Estrada, Eur. Phys. J. C **49**, 1011 (2007) [arXiv:hep-ph/0609255].
- [16] J. W. Chen, Y. H. Li, Y. F. Liu and E. Nakano, "QCD Viscosity to Entropy Density Ratio in the Hadronic Phase," arXiv:hep-ph/0703230.
- [17] A. Muronga, Phys. Rev. C **69**, 044901 (2004) [arXiv:nucl-th/0309056].
- [18] S. Muroya and N. Sasaki, Prog. Theor. Phys. **113**, 457 (2005) [arXiv:nucl-th/0408055].
- [19] S. Chapman and T.G. Cowling, "The Mathematical Theory of Non-uniform Gases, Third edition" (Cambridge, 1970)
- [20] S. Weinberg, Physica A **96**, 327 (1979).
- [21] N. Fettes, U. G. Meissner and S. Steininger, Nucl. Phys. A **640**, 199 (1998) [arXiv:hep-ph/9803266].
- [22] A. Sitenko and V. Tartakovskii, "Theory of Nucleus" (Kluwer, Netherlands, 1997)
- [23] P. Gerber, H. Leutwyler, and J.L. Goity, Phys. Lett. B246 (1990) 513.
- [24] P. Danielewicz and M. Gyulassy, Phys. Rev. D **31**, 53 (1985).
- [25] E. H. Kennard, "Kinetic Theory of Gases, with an Introduction to Statistical Mechanics" (McGraw-Hill, New York, 1938).
- [26] R. A. Lacey *et al.*, Phys. Rev. Lett. **98** (2007) 092301 [arXiv:nucl-ex/0609025].
- [27] J. B. Natowitz *et al.*, Phys. Rev. C **65**, 034618 (2002) [arXiv:nucl-ex/0106016], J. B. Elliott *et al.* [EOS Collaboration], Phys. Rev. C **67**, 024609 (2003) [arXiv:nucl-ex/0205004], L. G. Moretto, J. B. Elliott and L. Phair, Phys. Rev. C **72**, 064605 (2005) [arXiv:nucl-ex/0507015].
- [28] G. Colangelo, J. Gasser and H. Leutwyler, Nucl. Phys. B **603**, 125 (2001) [arXiv:hep-ph/0103088].
- [29] P. Baireyre, C. Bricman and G. Villet, Phys. Rev. 165 (1968) 1730, R. Koch and E. Pietarinen, Nucl. Phys. B 336 (1980) 331.
- [30] T. Ericson and W. Weise, "Pions and Nuclei" (Clarendon, Oxford, 1988)
- [31] Experimental data of nucleon-nucleon scattering are available from online at <http://nn-online.org/>
- [32] One can evaluate  $\langle\sigma\rangle$  by its thermal average similarly as in Eq. (26), but the qualitative behavior is the same as  $\sigma(\bar{p}(T))$ .
- [33] One can try to determine the values of  $T_c$  from the slope of each curve as in the pion gas case, but we do not perform such extrapolation for two reasons: First, it is practically very difficult to obtain reliable results since the highest temperature allowed for the Boltzmann equations gradually decreases with increasing  $\mu$ , as shown in Fig. 8. Second, the chiral phase transition at moderate values of  $\mu$  will be most likely of the first order, for which the ratio will show a discontinuity and the slope will not necessarily zero at  $T_c$ . Position of the critical end point may be detected from the behavior of the ratio  $\eta/s$  [26], but we do not expect our Boltzmann equations can describe the precise structure of the phase transition. We will discuss similar problems in relation to the nuclear liquid-gas phase transition in Sect.III.B.4.
- [34] Notice that all the examples (except for the QCD phase transition) discussed in Ref. [6] are about the liquid-gas phase transitions.